

Superconducting Phases in Lithium Decorated Graphene LiC_6

Rouhollah Gholami¹, Rostam Moradian^{1,2,*}, Sina Moradian³, and Warren E. Pickett⁴

¹Physics Department, Faculty of Science Razi University, Kermanshah, Iran

²Nano science and nano technology research center, Razi University, Kermanshah, Iran

*Correspondence and requested materials should be addressed to R. M. [rmoradian@raz.ac.ir]

³Department of Electrical and Computer Engineering, University of Central Florida, Orlando, Florida, USA.

⁴Department of Physics UC Davis, One Shield Avenue, Davis, CA 95616, USA.

ABSTRACT

A study of possible superconducting phases of graphene has been constructed in detail. A realistic tight binding model, fit to ab initio calculations, accounts for the Li-decoration of graphene with broken lattice symmetry, and includes s and d symmetry Bloch character that influences the gap symmetries that can arise. The resulting seven hybridized Li-C orbitals that support nine possible bond pairing amplitudes. The gap equation is solved for all possible gap symmetries. One band is weakly dispersive near the Fermi energy along $\Gamma \rightarrow M$ where its Bloch wave function has linear combination of $d_{x^2-y^2}$ and d_{xy} character, and is responsible for $d_{x^2-y^2}$ and d_{xy} pairing with lowest pairing energy in our model. These symmetries almost preserve properties from a two band model of pristine graphene. Another part of this band, along $K \rightarrow \Gamma$, is nearly degenerate with upper s band that favors extended s wave pairing which is not found in two band model. Upon electron doping to a critical chemical potential $\mu_1 = 0.22\text{eV}$ the pairing potential decreases, then increases until a second critical value $\mu_2 = 1.3\text{ eV}$ at which a phase transition to a distorted s -wave occurs. The distortion of d - or s -wave phases are a consequence of decoration which is not appear in two band pristine model. In the pristine graphene these phases convert to usual d -wave or extended s -wave pairing.

1 Introduction

Two dimensional superconducting phases have become of great interest since the discovery of the high temperature superconducting (HTS) cuprates and subsequent finding of Fe-pnictide and -chalcogenide HTSs. Interest was re-invigorated by the discovery of superconductivity onsets up to 75K in single layer FeSe grown on SrTiO_3 and related substrates.^{1,2} With the enormous research activity focused on graphene in recent years, it is not surprising that graphene-based superconductivity has become an active area of research. Very recently superconductivity up to 1.7K has been reported³ in magic angle bilayer graphene, which will buttress activity on two dimension superconductors and especially the related type that we discuss here.

Superconductivity has been known for some time in intercalated graphite compounds such as C_6Ca and C_6Yb ⁴. With the many remarkable properties of graphene, it has been anticipated that doping by gating or by decorating with electro-positive elements, thereby moving the chemical potential away from the Dirac points, might induce superconductivity. However, graphene decorated with alkali metals has three valence bands with one weakly dispersive band near Fermi energy. Due to this flat band, there are additional available states around the Fermi level and the required pairing potential is reduced.

Discussion of superconductivity in doped graphene has been primarily within theoretical models, as we review below, but some encouraging data have been reported. Experimental evidence for a superconducting gap in Li-decorated monolayer graphene around 6 K has been reported by Ludbrook *et al.* based on angle-resolved photoemission spectroscopy⁵ (ARPES). Scanning tunneling spectroscopy (STS) was applied by Palinkas *et al.*⁶ to graphene suspended on tin nanoparticles, who concluded that superconductivity is induced in the graphene layer. Evidence of superconductivity in Li-decorated few layer graphene at 7.4 K has been reported by Tiwari and collaborators⁷. Low temperature mobility of K and Li atoms on graphene was observed by Woo *et al.*, and suggest that mobility may persist at lower temperatures,⁸ which would provide new challenges for theory.

Various mechanisms of pairing have been proposed. Uchoa and Castro-Neto modeled pristine and doped graphene with electron-phonon coupling or plasmon mediated in mind⁹. Repulsive electron-electron interactions were modeled by Nandkishore and collaborators.^{10,11} Beginning from pristine graphene, varying the chemical potential leads to dominant chiral singlet $d_{x^2-y^2} + id_{xy}$ pairing for nearest neighbor interaction, according to Black-Schaffer *et al.*¹² a triplet f -wave state has been proposed to arise from next-nearest neighbor interaction with chemical potential near van Hove peak.¹³ Both chiral and conventional p -wave states in graphene have been discussed¹⁴, with the many pictures raising various possibilities but little of

a certain nature.

More specific predictions have begun to appear. Profeta *et al.* predicted¹⁵ based on Eliashberg theory that decoration by electron donating atoms such as Ca and Li would make single layer graphene superconducting, with modest critical temperatures in the 1-8 K range. In somewhat related work, Wong *et al.* have predicted¹⁶ from an ab initio treatment a critical temperature around $T_c=14\text{K}$ for carbon nanotubes, which was increased to above 100 K for a certain type of carbon ring.

Expectations of adjusting the chemical potential include gating, but the main focus has been on decoration of graphene by electropositive atoms, viz. alkalis or alkaline earths. Charge migration from such decorating atoms to the graphene layer will affect the C-C bonding, leading to contraction or expansion of the graphene hexagons that are centered by the decorating atoms, thus breaking the symmetry of C-C hopping integrals around the honeycomb loop. This asymmetric graphene layer will be referred to in this paper as “shrunk graphene”. Taking LiC_6 for illustration, each cell site has six C atoms in a hexagon with an alkaline atom lying above the center of the hexagon. The C π orbitals and alkaline atom’s s -orbital hybridize to give seven “molecular” orbitals. For two dimensional graphene-like structures effects, differences in nearest neighbour hopping integrals affect the band structure near the important Dirac point, which is folded back to the Γ point of the shrunk graphene superlattice investigated by Hou *et al.*¹⁷ and Long-Hua *et al.*¹⁸. For such systems not even the full analytic tight-binding band structure has yet been reported. The intent here is to extend study of this system, with representative LiC_6 , from the underlying electronic structure to investigation of the possible superconducting phases.

The organization of the paper is as follows. In Sec. II the interacting seven orbital model Hamiltonian is presented. The exact band structure of the normal state of this shrunk graphene system is described in Sec. III. Perturbation theory is applied to obtain the band structures in analytic form. Applying the Hubbard model and minimizing free energy of the superconductor state, we obtain in Sec. IV the gap equations and approximate critical temperature. These equations are solved analytically to establish the possible pairing symmetries and other properties of the superconducting states. A summary is provided in Sec. V.

2 Model Hamiltonian

Because the unit cell contains several atoms with important specific aspects, we provide many of the details of the expressions that can be obtained analytically. LiC_6 , as illustrated in Fig. 1, consists of a graphene layer decorated by a lithium layer in which Li atoms are located at the center of a carbon hexagon surrounded by six empty center hexagons. The height of Li above the carbon layer is calculated to be $h_z = 1.85$, somewhat smaller than the value 1.93\AA obtained by Profeta *et al.*¹⁵. The nearest Li-C distances are $h = 2.40$. Since the Li $2s$ orbital energy is higher than the C $2p_z$ orbital, charge transfer occurs. It is calculated that $0.685e$ from Li transfers to the six C atoms equally.¹⁹ The positive Li ion and negative C ion provide a relative Coulomb (Madelung) shift in site potentials of the two atoms.

The attractive interaction between Li and C ions after charge transfer contracts the Li-C distance and reduces the C-C bond lengths in the Li-centered hexagon to $a_1 = 1.425$, while the bond length of nearest neighbor C atoms in different hexagons is slightly larger at $a_2 = 1.426$. For Ca instead of Li, this difference should be larger, hence we keep these lengths distinct. The hopping integral between short-bond carbons is t_1 , with that between stretched carbon sites is denoted t'_1 . We refer to this broken symmetry situation as “shrunk graphene”. The difference in hopping amplitudes indicates that the new Li-C hopping parameter is the central new feature in LiC_6 compared to graphene. Symmetry breakdown leads to the opening of a small energy gap at the Γ point.

The lattice then becomes a two dimensional hexagonal Bravais lattice with seven atomic sites. These will be labeled as $A_1, A_2, A_3, B_1, B_2, B_3$ and Li , as illustrated in Fig. 1. The Hamiltonian of this system is

$$\hat{H} = - \sum_{i\alpha} \sum_{j\beta, \sigma} t_{i\alpha, j\beta}^{\sigma, \sigma} \hat{c}_{i\alpha\sigma}^\dagger \hat{c}_{j\beta\sigma} + \sum_{i\alpha, \sigma} (\epsilon_{i\alpha} - \mu_0) \hat{n}_{i\alpha\sigma} + \frac{1}{2} \sum_{i\alpha, \sigma} \sum_{j\beta, \sigma'} U_{i\alpha, j\beta}^{\sigma, \sigma'} \hat{n}_{i\alpha\sigma} \hat{n}_{j\beta\sigma'} = \hat{H}_N + \hat{H}_P. \quad (1)$$

Here H_N and H_P denote the non-interacting and interaction Hamiltonians respectively. In these expressions α and β run over A_i, B_i and Li . Here $\hat{c}_{i\alpha\sigma}^\dagger, \hat{c}_{i\alpha\sigma}$ are creation and annihilation operators of an electron with spin σ on subsite α of i th lattice site, and $\hat{n}_{i\alpha\sigma} = \hat{c}_{i\alpha\sigma}^\dagger \hat{c}_{i\alpha\sigma}$ is the electron number operator. The noninteracting chemical potential is μ_0 and $t_{i\alpha, j\beta}$ is the hopping integral from the α site of i th cell to the β site of j th cell. We denote the on-site energy by ϵ_α .

The interaction stated above corresponds to an extended (negative U) Hubbard model, which allows a variety of phenomenological values to be chosen and studied. It is largely for this reason that we provide substantial detail of the underlying, non-interacting C-Li lattice and electronic structure. The interactions that we study are introduced in Sec. IV.

3 Normal state of LiC_6

Many studies of graphene rely on tight binding parametrization of the band structure. The early parametrization of Wallace²⁰ already employed both first and second neighbors. Extensions in various ways have followed,^{21,22} culminating in the applica-

tion of Wannier functions by Jung and MacDonald²³ to provide simple but realistic five parameter model and a more accurate but more involved 15 parameter model. Our aim in this section is to construct a realistic seven band model for distorted LiC₆, while also developing the formalism to allow exploration of superconducting phases once the interaction has been included.

The distortion of the graphene layer to shrunken graphene and the coupling to Li requires a considerable generalization of the underlying tight binding model Hamiltonian, and many of the details are relegated to appendices. The Hamiltonian of non-interacting LiC₆ is

$$\hat{H}_N = - \sum_{i\alpha} \sum_{j\beta, \sigma} t_{i\alpha, j\beta}^{\sigma, \sigma} c_{i\alpha\sigma}^\dagger c_{j\beta\sigma} + \sum_{i\alpha, \sigma} (\epsilon_{i\alpha} - \mu_o) \hat{n}_{i\alpha\sigma}. \quad (2)$$

Eq. 2 incorporates broken symmetries in the on-site energies, hopping integrals, and bond lengths. Here, it has been assumed that on site energies $\epsilon_{A_i} = \epsilon_A$ and $\epsilon_{B_i} = \epsilon_B$. It is diagonalized in terms of Bloch eigenfunction of the form Eq. A.2. In matrix representation, the equation for the coefficients becomes

$$\begin{pmatrix} \epsilon_0(\vec{k}) & d_{c1}(\vec{k}) & d_{c3}(\vec{k}) & d_{c2}(\vec{k}) \\ d_{c1}^*(\vec{k}) & \epsilon_1(\vec{k}) & \beta(\vec{k}) & \gamma(\vec{k}) \\ d_{c3}^*(\vec{k}) & \beta^*(\vec{k}) & \epsilon_1(\vec{k}) & \theta(\vec{k}) \\ d_{c1}^*(\vec{k}) & \gamma^*(\vec{k}) & \theta^*(\vec{k}) & \epsilon_1(\vec{k}) \end{pmatrix} \begin{pmatrix} d_{c1}^*(\vec{k}) & d_{c3}^*(\vec{k}) & d_{c2}^*(\vec{k}) \\ \tau_1(\vec{k}) & d_2(\vec{k}) & d_3(\vec{k}) \\ d_2(\vec{k}) & \tau_3(\vec{k}) & d_1(\vec{k}) \\ d_3(\vec{k}) & d_1(\vec{k}) & \tau_2(\vec{k}) \end{pmatrix} \begin{pmatrix} \mathcal{C}_0(E_i(\vec{k})) \\ \mathcal{C}_1(E_i(\vec{k})) \\ \mathcal{C}_2(E_i(\vec{k})) \\ \mathcal{C}_3(E_i(\vec{k})) \end{pmatrix} = E_i(\vec{k}) \begin{pmatrix} \mathcal{C}_0(E_i(\vec{k})) \\ \mathcal{C}_1(E_i(\vec{k})) \\ \mathcal{C}_2(E_i(\vec{k})) \\ \mathcal{C}_3(E_i(\vec{k})) \\ \mathcal{C}_4(E_i(\vec{k})) \\ \mathcal{C}_5(E_i(\vec{k})) \\ \mathcal{C}_6(E_i(\vec{k})) \end{pmatrix} \quad (3)$$

where $d_{ci}(\vec{k})$, $\epsilon_i(\vec{k})$, $\beta(\vec{k})$, $\theta(\vec{k})$, $\gamma(\vec{k})$, $d_i(\vec{k})$ and $\tau_i(\vec{k})$ functions are defined in supplementary materials Eqs. A.7, A.8, A.9, and A.10 respectively. For general \vec{k} vectors, it is challenging to obtain an exact analytical expression for the full Hamiltonian in Eq. 3 and it would not be transparent anyway. However, analytical expression for Eq. 3 can be achieved in two steps. Since hopping from Li atoms to nearest neighbor carbon sites t_1^{LiC} is small with respect to C-C nearest neighbor hopping t_1 , by first neglecting the lithium-carbon hopping $t_1^{LiC} \rightarrow 0$, first column and row of the Hamiltonian matrix in Eq. 3 are omitted, the remaining part given by Eq. B.1 is uncoupled shrunken graphene Hamiltonian which can be diagonalized exactly to obtain $E_{sh,n}$. Finally, Li-C coupling is taken into account by perturbation theory to obtain eigenvalues E_n , as presented in the appendices.

3.1 Uncoupled C₆ Dispersion Relations

By first neglecting the lithium-carbon hopping, $t_1^{LiC} \rightarrow 0$, the uncoupled shrunken graphene Hamiltonian given by Eq. B.1 can be diagonalized exactly. Even though Li-C hopping has been neglected but still remaining part of shrunken Hamiltonian in the most general case, include broken symmetries in the hopping integrals, bond lengths and on-site energies. The non trivial eigenvalues of uncoupled shrunken graphene Hamiltonian in general form are given by

$$E_{sh,ml}(t_i, \vec{\xi}_i, \vec{k}) = -\mu_o + \alpha(\vec{k}) + u_m \Pi_0(\vec{k}) + u_m^* \Pi_0^*(\vec{k}) + \frac{1}{2} \left[\epsilon_A + \epsilon_B + (-1)^l \sqrt{(\epsilon_A - \epsilon_B)^2 + 4w_m(\vec{k})} \right] \quad (4)$$

with details presented in supplementary materials Appendix B. However, the obtained equations are often complicated. To provide insight into the method, uncoupled shrunken graphene Hamiltonian can diagonalized in some particular cases. The Brillouin zone (BZ) of C₆ is one third of that of graphene, with the Dirac points folded back to the Γ point. In this mini-BZ, the two π bands of pristine graphene i.e. $E_{\pm} = \pm t_1 |\eta_0|$ folds to six branches as illustrated in Fig. 2. These branches are solutions of Eq. B.1 in the limited case of pristine which in the nearest neighbor approximation they are given by,

$$\begin{aligned} E_{\gamma}^{\pm}(\vec{k}) &= \pm t_1 |\eta_0(\vec{k})|, & \eta_0(\vec{k}) &= e^{i\vec{k} \cdot \vec{\delta}_1} + e^{i\vec{k} \cdot \vec{\delta}_2} + e^{i\vec{k} \cdot \vec{\delta}_3} \\ E_{\beta}^{\pm}(\vec{k}) &= \pm t_1 |\eta_1(\vec{k})|, & \eta_1(\vec{k}) &= e^{i\vec{k} \cdot \vec{\delta}_1} + e^{i\frac{4\pi}{3}} e^{i\vec{k} \cdot \vec{\delta}_2} + e^{i\frac{2\pi}{3}} e^{i\vec{k} \cdot \vec{\delta}_3} \\ E_{\alpha}^{\pm}(\vec{k}) &= \pm t_1 |\eta_2(\vec{k})|, & \eta_2(\vec{k}) &= e^{i\vec{k} \cdot \vec{\delta}_1} + e^{i\frac{2\pi}{3}} e^{i\vec{k} \cdot \vec{\delta}_2} + e^{i\frac{4\pi}{3}} e^{i\vec{k} \cdot \vec{\delta}_3}. \end{aligned} \quad (5)$$

Exact analytical solutions for pristine graphene wherein next neighbor hopping integrals are taken into account are presented in supplementary materials Eqs. B.7 and B.8. As shown in Fig. 2 one sees that $E_{\beta}^{\pm}(\vec{k})$ is weakly dispersive near the van Hove singularity at the saddle points M at 3/8 or 5/8 filling (0.25 electron per carbon doping), this band plays a major role in the formation of superconductivity in graphene. Also, one can observe that the band structure is four-fold degenerate at the charge neutral Dirac points. Solution of the Schrödinger equation for pristine graphene in the mini-BZ has another advantage: the Bloch-wave symmetry character of each branch can be distinguished. The Bloch coefficients of the branch

labeled by E_γ are of s -wave character, $C_{A_i} = (1, -1, -1)$ while for those labeled as E_α and E_β are of the form $d \pm id$ -wave i.e. $C_{A_i} = (1, e^{\pm i\frac{2\pi}{3}}, e^{\pm i\frac{4\pi}{3}})$ as illustrated in Fig. 2 and demonstrated in more detail in Appendix B, Eqs. B.4 and B.6. This becomes important when it is shown that different superconducting phases of graphene in a variety of doping regimes are due to electron pairing in each of these branches.

Decoration of graphene with metals reduces symmetries that lead to removal of bands degeneracy in some regions. While decoration causes expansion and contraction of bonds length in three inequivalent directions in the honeycomb lattice i.e. $|\vec{\tau}_i| \neq |\vec{\delta}_i|$, eigenenergies $E_{sh,ml}(t_i, \vec{\xi}_i, \vec{k})$ in Eq. 4 do not depend on the bond lengths $\vec{\tau}_i$ and $\vec{\delta}_i$ separately but are functions of LiC_6 lattice bases length $|\vec{\xi}_i| = |\vec{\tau}_i + 2\vec{\delta}_i|$, so symmetry breakdown of bond lengths does not break symmetries of bands. Symmetry reduction of hopping integrals removes degeneracies occurring in pristine graphene band structure, with the most important effect being to open a gap $E_g = 2|t'_1 - t_1|$ at the Dirac point which has been folded back to the Γ point. This gap arises from symmetry breaking of the nearest neighbor hopping and dose not affected by the other next neighbors hopping nor by the Li-C hopping integral. Comparison with DFT band structures gives $E_g = 0.36\text{eV}$. Another gap can arise at the Γ point because of symmetry breaking of on-site energies $\epsilon_A \neq \epsilon_B$, seen from Eq. 4. For the case $t_1 = t'_1$ the gap becomes $2|\epsilon_A - \epsilon_B|$. In Li decorated graphene that we consider here, all carbon on-site energies are equal so this type gap does not arise.

While for folded but pristine graphene Bloch wave solutions are pure s -wave or chiral $d \pm id$ -wave and there are no mixed states, when symmetries in hopping integrals are broken by decoration, Bloch functions are linear combinations of all these phases, Eq. B.6. Equation B.7 demonstrates that for a general \vec{k} all probabilities are equal in pristine graphene i.e. $|C_{A_i}(E_m)|^2 = |C_{B_i}(E_m)|^2 = \frac{1}{6}$. In shrunken graphene these probabilities are \vec{k} dependent and unequal in general. It will be seen that these small deviations influence the superconducting gap equation symmetries.

3.2 Coupled LiC_6 Dispersion Relations

Li-C hopping adds a perturbation term to the shrunken graphene Hamiltonian. Obtaining exact dispersions from Eq. 3 is very challenging, so perturbation theory is applied to obtain approximate solutions, as presented in Appendix C. However, to get some insight into effects of the coupling, Eq. 3 can be solved exactly at the Γ point. At $\vec{k}=0$ only the isolated Li band, $E_{Li,0}(0)$ and the lowest valance band, $E_{sh,6}(0)$, are mutually affected. The energies of these bands are, with $E_0(0) \equiv E_+$, $E_6(0) \equiv E_-$,

$$E_{\pm}(0) = \frac{1}{2} (E_{Li,0}(0) + E_{sh,6}(0)) \pm \sqrt{\frac{1}{4} [E_{Li,0}(0) - E_{sh,6}(0)]^2 + 6(t_1^{LiC})^2} \quad (6)$$

and other shrunk graphene bands given by (supplementary) Eq. B.5 remain unchanged. Comparing the fit results from DFT to these equations suggests that t_1^{Li-C} is in the 0.3-0.5 eV range, and other next neighbor hopping from Li atoms to C sites are negligible.

There are two critical points in the pure graphene band structure which are affected by decoration and become important: the charge neutrality Dirac points folded at the Γ point, and the van Hove singularity at the M point. We define a hopping integral symmetry breaking index, $w_t = \frac{t'_1}{t_1} \neq 1$ indicates the degree of symmetry breaking. The difference in Li and C on-site energies can be considered to reflect the amount of doping. The Dirac points affected by w_t open a small gap E_g at Γ , which does not depend on t_1^{LiC} . Depending on doping level, Li-C hopping affects the band structure near the points that the isolated Li band $E_{Li,0}(\vec{k})$ and uncoupled shrunken graphene bands intersect. These impurity effects causes not only changes in energy level but alter the density of states. Superconductivity emerges from pairing of electrons near the Fermi energy and it is important to know how the density of states at the Fermi energy $N(0)$ changes with decoration.

3.3 Fitting of the seven-band tight binding model to DFT

The seven band tight binding model of LiC_6 was fit to the DFT band structure, with results illustrated in Fig. 3. In the graphene layer shown in Fig. 1(a) and (c), A_1 subsite chosen as central site labeled by 0 and B_1 subsite in adjacent hexagon considered as second neighbor while just slightly longer than the first neighbors atoms B_2 and B_3 in same hexagon, this neighbor labeled by $n = 2$ and so on the next neighbors are labeled. In Fig. 1 (a), the big dashed hexagon included up to nine neighbors but for the pristine graphene it is surrounded by five neighbors. C-C hopping from 0-subsite to n th neighbor has been shown by t_{0n}^{CC} . In-plane Li-Li hopping, t_{0m}^{LiLi} obtained up to $m = 4$ neighbors. Li to C hopping integrals are very small with respect to those of C-C and Li-Li, so we keep only the near neighbor Li-C hopping amplitude.

Since Li is small with respect to alkaline earths such as Ca, the pristine band structure is less affected by decoration by lithium than by calcium, as can be seen in Fig. 2 of Ref. [15]. The fitted hopping amplitudes and on-site energies are presented in Tables 1. Note that by comparing band structure of LiC_6 with pristine graphene in ref. [23], it is observed that Li decoration only slightly changes the pristine graphene band structure. These changes are due to electron transfer from Li to graphene, which changes the pristine on site $\epsilon_{pristine} = 0$ to $\epsilon_A = \epsilon_B = \epsilon_C$.

4 Superconducting Pairing and States

4.1 Bogoliubov-de Gennes Transformation

LiC₆ presents a multiband system in which three bands cross the Fermi level. We presume singlet pairing that can be both intraband and interband in nature. We adopt a local viewpoint in which pairing occurs between electrons on carbon atoms. Seven hybridized Li-C orbitals, support nine possible bond pairing amplitudes in real space. Figure 4 (a) illustrates all the nearest neighbour order parameters possibilities. Leaving the analytical derivation details to supplementary materials Appendices D and E, the quasiparticle energies are obtained by Bogoliubov-de Gennes unitary transformation in the seven band space,

$$E_{m,s}^Q(\vec{k}) = s \left(E_m(\vec{k}) + \sum_{i=1}^7 \frac{|\Delta_{mi}(\vec{k})|^2}{E_m(\vec{k}) + E_i(\vec{k})} \right) \quad s = \pm 1 \quad (7)$$

in which $s = 1$ is for particles and $s = -1$ for holes, and E_m are the normal state eigenvalues. The \vec{k} -dependent gap $|\Delta_{mi}(\vec{k})|^2$ in the spectrum are expressed as

$$\Delta_{mn}(\vec{k}) = \sum_{\alpha=1}^9 \Omega_{mn}^{\alpha}(\vec{k}) \Delta^{\alpha} \quad (8)$$

in which m and n are band indexes. The band pair order parameter $\Delta_{mn}(\vec{k})$ denotes pairing between electrons in the m -th and n -th bands in LiC₆. Also, $(\Delta^1, \Delta^2, \Delta^3) = (\Delta_1', \Delta_2', \Delta_3')$; $(\Delta^4, \Delta^5, \Delta^6) = (\Delta_1, \Delta_2, \Delta_3)$; $(\Delta^7, \Delta^8, \Delta^9) = (\Delta_1', \Delta_2', \Delta_3')$ are shown in Fig. 4(a), and

$$\begin{aligned} \Omega_{ij}^1(\vec{k}) &= \mathcal{C}_1^*(E_i) \mathcal{C}_4(E_j) e^{i\vec{k} \cdot \vec{\tau}_1} + \mathcal{C}_4^*(E_i) \mathcal{C}_1(E_j) e^{-i\vec{k} \cdot \vec{\tau}_1} \\ \Omega_{ij}^2(\vec{k}) &= \mathcal{C}_3^*(E_i) \mathcal{C}_6(E_j) e^{i\vec{k} \cdot \vec{\tau}_2} + \mathcal{C}_6^*(E_i) \mathcal{C}_3(E_j) e^{-i\vec{k} \cdot \vec{\tau}_2} \\ \Omega_{ij}^3(\vec{k}) &= \mathcal{C}_2^*(E_i) \mathcal{C}_5(E_j) e^{i\vec{k} \cdot \vec{\tau}_3} + \mathcal{C}_5^*(E_i) \mathcal{C}_2(E_j) e^{-i\vec{k} \cdot \vec{\tau}_3} \\ \Omega_{ij}^4(\vec{k}) &= \mathcal{C}_2^*(E_i) \mathcal{C}_6(E_j) e^{i\vec{k} \cdot \vec{\delta}_1} + \mathcal{C}_6^*(E_i) \mathcal{C}_2(E_j) e^{-i\vec{k} \cdot \vec{\delta}_1} \\ \Omega_{ij}^5(\vec{k}) &= \mathcal{C}_1^*(E_i) \mathcal{C}_5(E_j) e^{i\vec{k} \cdot \vec{\delta}_2} + \mathcal{C}_5^*(E_i) \mathcal{C}_1(E_j) e^{-i\vec{k} \cdot \vec{\delta}_2} \\ \Omega_{ij}^6(\vec{k}) &= \mathcal{C}_3^*(E_i) \mathcal{C}_4(E_j) e^{i\vec{k} \cdot \vec{\delta}_3} + \mathcal{C}_4^*(E_i) \mathcal{C}_3(E_j) e^{-i\vec{k} \cdot \vec{\delta}_3} \\ \Omega_{ij}^7(\vec{k}) &= \mathcal{C}_3^*(E_i) \mathcal{C}_5(E_j) e^{i\vec{k} \cdot \vec{\delta}_1} + \mathcal{C}_5^*(E_i) \mathcal{C}_3(E_j) e^{-i\vec{k} \cdot \vec{\delta}_1} \\ \Omega_{ij}^8(\vec{k}) &= \mathcal{C}_2^*(E_i) \mathcal{C}_4(E_j) e^{i\vec{k} \cdot \vec{\delta}_2} + \mathcal{C}_4^*(E_i) \mathcal{C}_2(E_j) e^{-i\vec{k} \cdot \vec{\delta}_2} \\ \Omega_{ij}^9(\vec{k}) &= \mathcal{C}_1^*(E_i) \mathcal{C}_6(E_j) e^{i\vec{k} \cdot \vec{\delta}_3} + \mathcal{C}_6^*(E_i) \mathcal{C}_1(E_j) e^{-i\vec{k} \cdot \vec{\delta}_3}. \end{aligned} \quad (9)$$

where $\mathcal{C}_i(E_j)$ are Bloch wave coefficients of the j -th band. Possible order parameter symmetries in Eq. 8 are related to symmetries of Bloch wave functions, through $\Omega_{ij}(\vec{k})$ functions in Eq. 9. In the limiting case of (folded) six band pristine graphene, the symmetry character of different conduction bands along high symmetry lines were provided in Fig. 2. Bloch symmetry character of non-interacting bands specifies the symmetry of the band order parameter.

4.2 Superconducting States

The linearized gap equation, obtained by minimizing the quasiparticle free energy with respect to nearest neighbor order parameters, is

$$J_{\beta} \Delta^{\beta} = -\frac{1}{2N} \sum_{\alpha=1}^9 \left[\sum_{\vec{k}} \sum_{n=1}^7 \sum_{i=1}^7 \frac{\tanh(\frac{E_n^Q}{2k_B T})}{E_n(\vec{k}) + E_i(\vec{k})} \left(\Omega_{ni}^{\alpha}(\vec{k}) \Omega_{ni}^{*\beta}(\vec{k}) + \Omega_{ni}^{\beta}(\vec{k}) \Omega_{ni}^{*\alpha}(\vec{k}) \right) \right] \Delta^{\alpha} \equiv -\sum_{\alpha=1}^9 \Gamma_{\beta\alpha} \Delta^{\alpha}. \quad (10)$$

This equation can be written in matrix form as

$$\begin{bmatrix} A_{3 \times 3} & B_{3 \times 3} & B_{3 \times 3} \\ B_{3 \times 3} & C_{3 \times 3} & D_{3 \times 3} \\ B_{3 \times 3} & D_{3 \times 3} & C_{3 \times 3} \end{bmatrix} \begin{pmatrix} g_1 V_1 \\ g_0 V_2 \\ g_0 V_3 \end{pmatrix} = - \begin{pmatrix} V_1 \\ V_2 \\ V_3 \end{pmatrix} \quad (11)$$

where

$$A_{3 \times 3} = \begin{bmatrix} \Gamma_{11} & \Gamma_{12} & \Gamma_{12} \\ \Gamma_{12} & \Gamma_{11} & \Gamma_{12} \\ \Gamma_{12} & \Gamma_{12} & \Gamma_{11} \end{bmatrix}, C_{3 \times 3} = \begin{bmatrix} \Gamma_{44} & \Gamma_{45} & \Gamma_{45} \\ \Gamma_{45} & \Gamma_{44} & \Gamma_{45} \\ \Gamma_{45} & \Gamma_{45} & \Gamma_{44} \end{bmatrix}, B_{3 \times 3} = \begin{bmatrix} \Gamma_{14} & \Gamma_{15} & \Gamma_{15} \\ \Gamma_{15} & \Gamma_{14} & \Gamma_{15} \\ \Gamma_{15} & \Gamma_{15} & \Gamma_{14} \end{bmatrix}, D_{3 \times 3} = \begin{bmatrix} \Gamma_{47} & \Gamma_{48} & \Gamma_{48} \\ \Gamma_{48} & \Gamma_{47} & \Gamma_{48} \\ \Gamma_{48} & \Gamma_{48} & \Gamma_{47} \end{bmatrix} \quad (12)$$

and $g_1 V_1 = (\Delta_1'' \Delta_2'' \Delta_3'')^T$, $g_0 V_2 = (\Delta_1 \Delta_2 \Delta_3)^T$ and $g_0 V_3 = (\Delta_1' \Delta_2' \Delta_3')^T$; the subscripts $\langle ij \rangle$ has been dropped for brevity. The $A_{3 \times 3}$, $B_{3 \times 3}$, $C_{3 \times 3}$, and $D_{3 \times 3}$ matrices, given by Eq. 12, have identical structures, hence they share eigenvectors: $V_s^T = (1 \ 1 \ 1)$, $V_{d_{xy}}^T = (1 \ -1 \ 0)$, and $V_{d_{x^2-y^2}}^T = (1 \ 1 \ -2)$, where the latter two are degenerate. Their eigenvalues, in obvious notation, are

$$\begin{aligned} a_s &= \Gamma_{11} + 2\Gamma_{12}, \quad b_s = \Gamma_{14} + 2\Gamma_{15}, \quad c_s = \Gamma_{44} + 2\Gamma_{45}, \quad d_s = \Gamma_{47} + 2\Gamma_{48} \\ a_d &= \Gamma_{11} - \Gamma_{12}, \quad b_d = \Gamma_{14} - \Gamma_{15}, \quad c_d = \Gamma_{44} - \Gamma_{45}, \quad d_d = \Gamma_{47} - \Gamma_{48}. \end{aligned} \quad (13)$$

For folded six band pure graphene $g_0 = g_1$, the Bloch wave coefficients appearing in Eq. 9 can be replaced from Eq. B.7 to show that $\Omega_{ij}^1(\vec{k}) = \Omega_{ji}^7(\vec{k}) = \Omega_{ij}^7(\vec{k})$ and similarly relations for other elements, hence $C_{3 \times 3} = A_{3 \times 3}$ and $D_{3 \times 3} = B_{3 \times 3}$. Eq. 11 takes the more symmetric form

$$\begin{bmatrix} A_{3 \times 3} & B_{3 \times 3} & B_{3 \times 3} \\ B_{3 \times 3} & A_{3 \times 3} & B_{3 \times 3} \\ B_{3 \times 3} & B_{3 \times 3} & A_{3 \times 3} \end{bmatrix} \begin{pmatrix} V_1 \\ V_2 \\ V_3 \end{pmatrix} = -\frac{1}{g_0} \begin{pmatrix} V_1 \\ V_2 \\ V_3 \end{pmatrix} \quad (14)$$

For the case $V_1 = V_2 = V_3 = V_{sy}$ where sy subscripts indicates each of the s , d_{xy} or $d_{x^2-y^2}$ symmetry, the six band gap Eq. 14 reduces to $(A + 2B)V_{sy} = -\frac{1}{g_0}V_{sy}$, i.e. the linearized gap equation of the two band model of pristine graphene in Ref. [12]. These three solutions preserve symmetry of the two band unit cell as illustrated in Fig. 4 (b), (c). In addition to these three states, there are six more non-orthogonal solutions $\Phi_{0n} = (V_{sy} \ 0 \ -V_{sy})$ and $\Phi_{1n} = (V_{sy} \ -V_{sy} \ 0)$ that break symmetries of pristine graphene two band model. Inserting these solutions into Eq. 14 leads to a new two band gap equation, $(A - B)V_{sy} = -\frac{1}{g_0}V_{sy}$, which is unphysical because of an unreachably high energy pairing potential g_0 . In the following section the superconducting gap equation has been solved for LiC_6 and it is demonstrated how Li-C coupling influences superconducting phases.

4.3 Nine Superconducting Phases

Self-consistent solutions of the gap equation Eq. 11 can be obtained analytically. There are three superconducting states with island character (discussed in more detail below) that can be expressed in compact form as

$$[\Phi_n]^T = [0 \quad V_{sy} \quad -V_{sy}], \quad J_{sy}^0 = c_{sy} - d_{sy} \quad (15)$$

where V_{sy} refers to one of the V_s , $V_{d_{xy}}$ or $V_{d_{x^2-y^2}}$ -wave symmetries. Pairing in these phases cannot propagate, as may be pictured in Fig. 5. The other six superconducting states of Eq. 11 have the explicit form

$$[\Phi_n]^T = [\alpha_{sy}^\pm V_{sy} \quad V_{sy} \quad V_{sy}] \quad (16)$$

corresponding to the interaction potential is $g_0 = \frac{1}{J_{sy}}$ wherein

$$\alpha_{sy}^\pm = \frac{J_{sy}^\pm - c_{sy} - d_{sy}}{b_{sy}}, \quad J_{sy}^\pm = \frac{1}{2} \left(\kappa a_{sy} + c_{sy} + d_{sy} \pm \sqrt{8\kappa b_{sy}^2 + [c_{sy} + d_{sy} - \kappa a_{sy}]^2} \right) \quad (17)$$

In these expressions $J_{d(s)}^\pm$ and $\alpha_{d(s)}^\pm$ are obtained from Eq. 17 by substituting a_{sy} , b_{sy} , c_{sy} , and d_{sy} by $a_{d(s)}$, $b_{d(s)}$, $c_{d(s)}$, and $d_{d(s)}$ respectively.

By comparing the gap equations introduced in Eq. 11 and Eq. 14 the gap equation symmetry reduction of decorated graphene with respect to folded but pristine graphene becomes clear. This symmetry reduction results in an α_{sy} coefficient appearing in the pairing amplitudes of stretched bonds as shown in Eq. 16 and Fig. 4. We refer to these symmetry reduction phases as “distorted phases”.

The six bands of pristine graphene support nine pairing amplitudes while in the two band model there are three possible pairing amplitudes along three different bonds. These two notions can be mapped onto each other only if $\alpha_{sy} = 1$ as illustrated in Fig. 4(b),(c). Therefor the three island superconducting phases given by Eq. 15 in the special case of pristine cannot be mapped onto the two band model. These three phases are unphysical even in the case of decorated graphene because the Cooper pairs in these phases require a large pairing potential. In the special case of pristine graphene in which $\kappa = 1$, $a_{sy} = c_{cy}$ and $b_{sy} = d_{cy}$ from Eq. 17, and it follows that if $b_{sy} > 0$ then $\alpha_{sy}^+ = 1$ and $\alpha_{sy}^- = -2$. Also $g_0^+ < g_0^-$ so in this case (+) sign preserves the two band model while the (−) sign phases are unphysical. Numerical calculation shows that $b_{sy}^+ > 0$. These superconducting states can be categorized into three groups according to their corresponding pairing potential.

3 electron pairing states with island character and very high pairing potential; (unphysical solutions)

$$\begin{aligned}
\Phi_{p_x} &= \frac{1}{2} [(0\ 0\ 0) (1\ -1\ 0)(-1\ 1\ 0)]^T, \quad g_0 = \frac{1}{c_d - d_d}, \\
\Phi_{p_y} &= \frac{1}{2\sqrt{3}} [(0\ 0\ 0) (1\ 1\ -2)(-1\ -1\ 2)]^T, \quad g_0 = \frac{1}{c_d - d_d}, \\
\Phi_f &= \frac{1}{\sqrt{6}} [(0\ 0\ 0) (1\ 1\ 1)(-1\ -1\ -1)]^T, \quad g_0 = \frac{1}{c_s - d_s}.
\end{aligned} \tag{18}$$

3 states with higher electron pairing potential; (unphysical solutions)

$$\begin{aligned}
\Phi_{d_{x^2-y^2}}^- &= (6(\alpha_d^-)^2 + 12)^{-\frac{1}{2}} [\alpha_d^- (1\ -1\ -2) \ (1\ 1\ -2) \ (1\ 1\ -2)]^T, \quad g_0 = \frac{1}{J_d^-}, \\
\Phi_{d_{xy}}^- &= (2(\alpha_d^-)^2 + 4)^{-\frac{1}{2}} [\alpha_d^- (1\ -1\ 0) \ (1\ -1\ 0) \ (1\ -1\ 0)]^T, \quad g_0 = \frac{1}{J_d^-}, \\
\Phi_s^- &= (3(\alpha_s^-)^2 + 6)^{-\frac{1}{2}} [\alpha_s^- (1\ 1\ 1) \ (1\ 1\ 1) \ (1\ 1\ 1)]^T, \quad g_0 = \frac{1}{J_s^-}.
\end{aligned} \tag{19}$$

3 states with lower electron pairing potential; (physical solutions)

$$\begin{aligned}
\Phi_{d_{x^2-y^2}}^+ &= (6(\alpha_d^+)^2 + 12)^{-\frac{1}{2}} [\alpha_d^+ (1\ -1\ -2) \ (1\ 1\ -2) \ (1\ 1\ -2)]^T, \quad g_0 = \frac{1}{J_d^+}, \\
\Phi_{d_{xy}}^+ &= (2(\alpha_d^+)^2 + 4)^{-\frac{1}{2}} [\alpha_d^+ (1\ -1\ 0) \ (1\ -1\ 0) \ (1\ -1\ 0)]^T, \quad g_0 = \frac{1}{J_d^+}, \\
\Phi_s^+ &= (3(\alpha_s^+)^2 + 6)^{-\frac{1}{2}} [\alpha_s^+ (1\ 1\ 1) \ (1\ 1\ 1) \ (1\ 1\ 1)]^T, \quad g_0 = \frac{1}{J_s^+}.
\end{aligned} \tag{20}$$

All states are orthogonal except those with same subscript, viz. Φ_s^- and Φ_s^+ . Such solutions are orthogonal if $\kappa = 1$, *i.e.* $g_1 = g_0$. Only for this case the matrix gap equation becomes Hermitian, then band order parameters takes the following form in terms of the band Green function and g_0 ,

$$\Delta_{ij}(\vec{k}) = g_0 \langle d_i^\dagger(\vec{k}) d_j^\dagger(\vec{k}) \rangle. \tag{21}$$

Here $\hat{d}_i^\sigma(\vec{k}) = \sum_{m=1}^7 \mathcal{C}_m^*(E_i(\vec{k})) \hat{c}_m^\sigma(\vec{k})$ annihilates an electron with spin σ in the i th band with energy $E_i(\vec{k})$. Although it is assumed that $g_1 = g_0$ but deviation from pristine leads to distortion of Green's functions $\langle \hat{c}_{i\alpha}^\dagger \hat{c}_{j\beta}^\dagger \rangle$ along different bonds.

Phases $\Phi_{d_{x^2-y^2}}^-$ and $\Phi_{d_{xy}}^-$ are degenerate with eigenvalue $J_{d_{x^2-y^2}}^- = J_{d_{xy}}^- = J_d^-$, and similarly $\Phi_{d_{x^2-y^2}}^+$ and $\Phi_{d_{xy}}^+$ with eigenvalue J_d^+ . For Li decorated graphene, numerical calculation shows $J_{sy}^+ > J_{sy}^-$, so g_0 in the (+) states is lower than g_0 in the (−) states hence pairing in this modes are dominant. From Eqs. 19 and 20 we observe that probability amplitudes for pairing on different bonds in real space differ for the various states. For the long C-C bonds the probability is proportional to $(\alpha_{sy}^\pm)^2$ while for the others is unity. Numerical results are shown in Fig. 6.

5 Discussion And Relation To Previous Work

The possibility of a superconductivity state in metal decorated graphene has been suggested theoretically by a few groups.^{9,12,15} Some have suggested phonon-mediated superconductivity in single layer graphene. Most prominently, Profeta *et al.*¹⁵ calculated on the basis of density functional theory for superconductors that decoration by electron donating atoms such as Ca and Li will make single layer graphene superconducting, up to 8K for the case of Li. The *ab initio* anisotropic Migdal-Eliashberg formalism was used by Zheng and Margine²⁴, who predicted a single anisotropic superconducting gap with critical temperature $T_c = 5.1 - 7.6K$, in surprisingly good agreement with experimental reported superconductivity around 6K in LiC_6 .⁵

Using a phenomenological microscopic Hamiltonian in a nearest-neighbor tight-binding approximation, possible superconducting phases of pristine graphene have been discussed by Uchoa and Castro-Neto⁹ and also by Black-Schaffer and Doniach¹². The possibility of a singlet $p + ip$ phase pairing near the Dirac points between nearest neighbors subsites were suggested by Uchoa and Castro-Neto⁹. They worked in terms of a plasmon mediated mechanism for metal coated graphene, and discussed the conditions under which attractive electron-electron interaction can be mediated by plasmons.

Singlet superconducting gap phases of pristine graphene have been proposed and discussed by Black-Schaffer and Doniach.¹² For the nearest neighbors pairing amplitudes $\Delta_{\langle iA|jB\rangle} = \Delta_{iA,iA+\vec{\delta}_j}$ where $\vec{\delta}_j$ are the vectors that connects the iA site to its three nearest neighbors, it was observed that there are three states that minimize the free energy in various regimes of the parameters, which here have been denoted by $V_s = (1, 1, 1)^T$, $V_{d_{x^2-y^2}} = (2, -1, -1)^T$, and $V_{d_{xy}} = (0, -1, 1)^T$. Pairing symmetries d_{xy} and $d_{x^2-y^2}$ are degenerate, and only the linear combination of $d_{x^2-y^2} + id_{xy} \equiv d + id$ preserves the graphene band symmetry. Depending on the position of the Fermi energy with respect to Dirac points, $d + id$ or s states tend to dominate. Their numerical calculation showed that d -wave solutions will always be favored for electron or hole doping in the regime $0 < \bar{n}_c < 0.4$ where doping is defined by $\bar{n}_\alpha = \langle \hat{c}_{i\alpha}^\dagger \hat{c}_{i\alpha} \rangle - 1$. In this regime, superconductivity can emerge from electronic correlation effects. Near the van Hove singularity at the saddle point M corresponding to $3/8$ and $5/8$ fillings i.e. $\bar{n}_c = 0.25$, it was suggested that chiral $d + id$ superconductivity, which breaks time-reversal symmetry, can be stabilized. In this regime d -wave superconductivity may arise from repulsive electron-electron interaction¹¹.

Although doping by a gate voltage is normally considered to change only the chemical potential but not the band structure, gating cannot be expected to push the Fermi energy to the van Hove singularity without altering the band dispersion. The most likely way to do this is by decoration with electropositive atoms, which has been our focus. We note that doping is essential, when graphene decorated, in addition to the expected charge migration from the decorating atoms to the graphene sheet, it is then necessary the interlayer state is partially occupied to induce superconductivity as happens in GICs. Hybridization of interlayer s -band and graphene π bands changes the graphene band structure. The s orbitals of Ca have more overlap with C orbitals than Li and lead to stronger and longer range interactions as well as increasing the doping level, effects that become detrimental to superconductivity. For this reason our emphasis here is on the Li decorated graphene.

We review some of our main points. When graphene is decorated by Li, electron transfer from Li atoms to C contracts the Li-C distance and reduces the C-C bond lengths in the Li-centered hexagon. In this kekulé-type structure, hopping amplitude symmetries of all C-C neighbors are broken (our “shrunk graphene”). This model allows study of multiband effects on the superconducting phase diagram. To gain insight into our model, solutions of superconducting gap equation in both cases of folded bands otherwise pristine C_6 and the usual two band model of C_2 were compared. These two viewpoints coincide if the same pairing paradigms are considered. For pristine graphene with its two site cell, in real space picture electrons can pair with near neighbors in three inequivalent directions, $\Delta_{i,i+\vec{\delta}} = V_{sy} = (\Delta_1 \Delta_2 \Delta_3)^T$ which must respect honeycomb symmetries. The V_{sy} quantities are the three vectors that belong to the irreducible representation of crystal point group D_{6h} i.e. $V_{sy}^T = (1, 1, 1)$, $(-1, 1, 0)$ and $(2, -1, -1)$ for which the sy subscript stands for symmetries s , d_{xy} and $d_{x^2-y^2}$. Permutation of s -wave solution $(1, 1, 1)$ along three different bonds constructs just one state while permutation of d_{xy} solution $(-1, 1, 0)$ up to a minus sign constructs two nonorthogonal linear independent states viz. $(-1, 1, 0)$ and $(-1, 0, 1)$ which orthogonal linear combination of them are $d_{xy}^T = (-1, 1, 0)$ and $d_{x^2-y^2}^T = (2, -1, -1)$.

A similar procedure again can be applied to pristine graphene but now in enlarged six site unit cell. Unit cell of C_6 includes six carbon subsites and nine different bonds that support nine possible nearest neighbor bond pairing amplitudes as illustrated in Fig. 4 and denoted them by $\Phi_{sy}^T = [(\Delta_1'', \Delta_2'', \Delta_3'')(\Delta_1^1, \Delta_2^2, \Delta_3^3)(\Delta_1', \Delta_2', \Delta_3')]$. The gap equation is a 9×9 matrix equation given by Eq. 14. The folded bands supercell include three vertices numbered 5, 6, 7, and nine bonds as shown in Fig. 4(a). There are nine orthogonal solutions that preserve symmetries of this supercell. One of these configurations has s -wave symmetry $(1, 1, 1, 1, 1, 1, 1, 1, 1)$ the other eight solutions are constructed by all possible permutations of $(-1, 1, 0)$ along these bonds that preserve our supercell symmetry. There are only three solutions which can preserve symmetry of both two and six atoms cells simultaneously which they are of the form $\Phi_{sy}^+ = (V_{sy} V_{sy} V_{sy})^T$ as illustrated in Fig. 4. For these solutions, the folded 9×9 gap equation reduces to 3×3 gap equations of ordinary pristine graphene. The Cooper pair formation energy for these three modes are significantly less than the other six phases which are not reducible to the two band model.

In fact reduction of symmetry leads to increasing of the system free energy. After the orthogonalization procedure, one obtains three solutions Φ_f , Φ_{p_x} and Φ_{p_y} , of the form $\Phi_{sy}^0 = (0 \ V_{sy} \ -V_{sy})^T$. These phases have been designated as island phases, as illustrated in Fig. 5(b) for Φ_f , within which a pairing amplitude is localized within island hexagons and cannot propagate. For these island phases, numerical calculation of the electron pair potential energy g_0 shows that g_0 is large. This kind of solutions is a consequence of the six atom basis and does not appear for the two atom basis. Also, there are three solutions of the form $\Phi_{sy}^- = (-2V_{sy} V_{sy} V_{sy})^T$ which also break symmetry of two atom cell. For these reasons, in association with the normal state band structure of graphene, we concentrate on superconductivity in the three Φ_{sy}^+ symmetry phases.

For pristine graphene C_2 , two normal bands are $E_\pm = \pm t_1 |\eta_0|$ which fold to six branches in mini-BZ of C_6 i.e. $E_\gamma^\pm = \pm t_1 |\eta_0|$, $E_\beta^\pm = \pm t_1 |\eta_1|$ and $E_\alpha^\pm = \pm t_1 |\eta_2|$ as shown in figure:eta-k, also Bloch-wave symmetry character of each branch has been distinguished. The Bloch coefficients of the branch labeled by γ are of s -wave character, $C_{A_i} = (1, 1, 1)$ and for those labeled as α and β are of the form $d \pm id$ type, i.e. $C_{A_i} = (1, e^{\pm i \frac{2\pi}{3}}, e^{\pm i \frac{4\pi}{3}})$. Based on Bloch wave character of these branches one can obtain the dominant superconducting phases of pristine graphene in various doping regimes. d -wave pairing emerges from the d -wave branches of the folded band structure E_α^\pm and E_β^\pm , while s -wave pairing arises from the s -wave branch E_γ^\pm .

For folded but otherwise pristine graphene, Fig. 2 illustrates that the lowest conduction band, weakly dispersive along $\Gamma \rightarrow M$, is responsible for dominant singlet superconductivity in chiral $d \pm id$ symmetry. Upon electron doping to the critical vHs at $\bar{n}_c = 0.25$, the pairing potential g_0 in the $d \pm id$ phase decreases, beyond which density of states decreases. g_0 increases until a second critical value of doping $\bar{n}_c = 0.4$ at which a phase transition to s -wave pairing occurs. Bloch states in higher conduction bands include combinations of s and f symmetries that favor extended s wave pairing. The multiband character is responsible for stabilizing singlet s superconductivity at high electron or hole doping.

To understand how superconducting phases of graphene can be affected by decoration by Li, one can compare the LiC₆ gap solutions with those of folded bands C₆ at the same doping. Numerical results for pristine graphene gap equation performed in the nearest neighbor approximation in Ref.¹² have been extended by applying a more accurate tight binding model fit to the DFT band structure of pristine graphene²³. Although a quantum critical point for zero doping reported by Black-Schaffer and Doniach¹² at dimensionless coupling $\frac{g_0}{t} = 1.91$ which d - and s -wave solutions are degenerate. In the more realistic tight binding model we applied, this degeneracy is not observed at the Γ point, and the d -wave solution is dominant. This difference may be consequence of particle-hole symmetry breaking of valence and conduction bands. Also the van Hove singularity at the M point is moved from 0.25 doping for nearest neighbor hopping to 0.16 doping in the accurate model. The phase transition from d -wave to s -wave is shifted to 0.35 doping instead of the 0.4 doping reported for nearest neighbor hopping.¹² Numerical calculations for this more detailed model are illustrated in Fig. 7.

When graphene is decorated by Li, around 0.68 electron per lithium atom transfers to neighboring C sites, viz. $\bar{n}_c = 0.11$, and the Dirac points folded to Γ move to -1.52 eV. Symmetry breaking of the hopping partially removes degeneracies of band structure of pristine graphene, which leads to creation of the small gap at Γ , with energy $E_g = 2|t_1 - t'_1| = 0.36\text{eV}$. Also two of four-fold degeneracies between valence and conduction bands at the Dirac points are removed. Compression between band structure of decorated graphene and folded pristine graphene at the same doping shows that hybridization of the Li s band and C π band is small. This means nearest neighbor Li-C hopping is in the range $t_1^{LiC} \sim 0.3 - 0.5$, and further hoppings are negligible.

Li decoration of graphene changes not only the band structure but also the Bloch wave coefficients from those of pristine graphene. While pristine graphene Bloch wave coefficients have pure s - or d -wave character and their magnitudes are \vec{k} -independent. In the case of LiC₆ they become mixed and vary with \vec{k} , hence gap equation symmetry is reduced. Because of this symmetry reduction, for the longer C-C bonds, a new coefficient α_{sy} appears in the pairing amplitudes. In terms of this coefficient we have classified superconducting phase symmetries into three groups. Eqs. 18, 19, and 20 present all nine possible pairing phases of LiC₆. There are three categories of solutions which have not appeared in complete form in the literature. The total of nine phases arise from spatial, and therefore hopping parameter, symmetry breaking.

In the first category Φ_f , Φ_{px} and Φ_{py} , there is $\alpha_{sy} = 0$ identical to that of folded pristine C₆. For the second category, α_{sy} (denoted by α^-) is negative, in the case of pristine $\alpha^- = -2$ as discussed. These three phases break the two site cell symmetry, and numerical calculation shows that the pairing potential g_0 must be large to realize these phases. For the last category α^+ is positive. Three phases which correspond to $\alpha^+ > 0$ include $\Phi_{d_{x^2-y^2}}^+$, $\Phi_{d_{xy}}^+$, and Φ_s^+ , and these have the lowest pairing potentials with respect to the other six phases.

In the limiting case of folded six band pristine graphene $\alpha_{d_{x^2-y^2}}^+$, $\alpha_{d_{xy}}^+$, and α_s^+ are all equal to unity, which maps the results to the two-band symmetries as it should. But when Li decorated, depending on doping strength viz. w_t and t_1^{LiC} these coefficients α_{sy}^+ no longer remain unity. The pairing amplitude distortion along longer C-C bonds α^+ , for s -wave phase is significant due to its spatial isotropic symmetry. In spite of the pristine nature this phase no longer preserves two band model symmetry. On the other hand, d -wave phases are hardly affected by doping and their superconductivity is more persistent against perturbation. The chirality or non-chirality of Cooper pairs in these phases is undetermined, however. As shown in Fig. 6(b), at low temperature $\alpha_s^+ \approx 0.6$ for Φ_s^+ , and $\alpha_{d_{x^2-y^2}}^+ = \alpha_{d_{xy}}^+ \equiv \alpha_d^+$ is approximately equal to unity and varies little with temperature.

At a given critical temperature T_c and chemical potential μ_0 , for each of nine possible superconducting phases, Eqs. 10, 13, and 17 were evaluated numerically over the BZ of LiC₆ to find the corresponding pairing potential $g_0 = \frac{1}{J_{sy}}$ and α_{sy} coefficient. Smaller g_0 means less Cooper pair formation energy is required. Fig. 6(a) provides the phase boundaries for T_c in terms of the pairing potential g_0 for LiC₆ in which $\mu_0 = 0$. For a given transition temperature T_c , by changing the chemical potential μ_0 of LiC₆ via gating, one can engineer the pairing potential g_0 . Figure 8 gives a g_0 - μ_0 phase boundary diagram at $T_c = 0.1$ K. As illustrated in this figure, similarly to pristine graphene, decoration with Li atoms makes it is possible to change the dominant pairing and to have a symmetry-change phase transition from d to “distorted s -wave.” Changing μ_0 up to $\mu_{o-v} \approx 0.22\text{eV}$ so that the distance between the Fermi energy and the saddle points decreases, leads to a decrease in g_0 . Continuously increasing μ_0 up to 0.5 eV causes g_0 to increase for both d -wave and “distorted s -wave” pairing, and after that a smooth decrease proceeds. For both symmetries at critical $\mu_{o-c} = 1.3$ eV mixed state exist.

Up to $\mu_{o-c} = 1.3$ eV, the flat band plays a primary role in formation of Cooper pairs with lowest energy. The Bloch wave

function of this band consists of d and p character, therefore Γ_{12} , Γ_{15} , Γ_{45} and Γ_{48} in Eq. 13 carry minus signs. This makes it evident from Eq. 17 that d -wave pairing is dominant. Beyond that, the uneven part of the “flat band” and also upper bands assume a major role. These bands consist of d , p , s , and f character Bloch wave functions (as defined in earlier sections) with a significantly low density of states. In this case Γ_{12} , Γ_{15} , Γ_{45} and Γ_{48} change their sign, hence s -wave pairing is favored.

Numerically we have demonstrated that electron pairing g_0 in the limit of pristine graphene is minimal for all dopings. Our calculations indicate that any perturbation of the flat band reduces T_c . The flat band can be perturbed through electron hopping from decorating atoms to carbon sites (t_1^{LiC}) or by hopping symmetry breaking index w_t . For fixed doping at $\bar{n} = 0.11$ electron per carbon site and for fixed $w_t = 0.94$ as obtained for lithium decorated, in a variety of Li-C hopping between 0.3-0.4eV, numerical calculation doesn't show significant altering of pair interaction potential g_0 in s - and d -wave phases. But, as one could see there is not an explicit behavior in a general coupling strength. A result is that a general aspect of superconducting pairing in LiC₆ and pristine graphene is almost the same in the $d_{x^2-y^2}$ and d_{xy} phases due to robustness of the flat band against perturbation.

To summarize, our calculations indicate that d -wave phases exist and are dominant symmetry of pairing in both pristine and Li decorated graphene. Pure s -wave phase does not appear in LiC₆, and s -wave superconductivity in metal decorated graphene is disfavored because of spatially increased overlap for s -wave symmetry. These results show that while degree of doping plays a major role in the graphene superconductivity, perturbation effects of decorating atoms finally determine the phase diagram. Our work also provides a new type of classification of superconducting phases in LiC₆-like nanostructures, and certain aspects of the formalism may be useful in modeling the recently observed superconductivity in magic angle bilayer graphene.³

References

1. Wang, Q. Y. *et al.* Interface-Induced High-Temperature Superconductivity in Single Unit-Cell FeSe Films on SrTiO₃. *Chin. Phys. Lett.* **29**, 037402 (2012).
2. He, S. L. *et al.* Phase diagram and electronic indication of high-temperature superconductivity at 65 K in single-layer FeSe films. *Nat. Mater.* **12**, 605 (2013).
3. Cao, Y. *et al.* Unconventional superconductivity in magic-angle graphene superlattices. *Nature* **556**, 43-50 (2018).
4. Weller, T. E. *et al.* Superconductivity in the intercalated graphite compounds C₆Yb and C₆Ca. *Nature Phys.* **1**, 39 (2005).
5. Ludbrook, B.M. *et al.* Evidence for superconductivity in Li-decorated monolayer graphene. *Proc. Natl. Acad. Sci. USA* **112**, 11795-11799 (2015).
6. Palinkas, A. *et al.* Novel graphene/Sn and graphene/SnO_x hybrid nanostructures: induced superconductivity and band gaps revealed by scanning probe measurements. *Carbon* **124**, 611 (2017).
7. Tiwari, A. P. *et al.* Superconductivity at 7.4K in few layer graphene by Li intercalation. *J. Phys.: Condens. Matt.* **29**, 445701 (2017).
8. Woo, S. *et al.* Temperature-dependent transport properties of graphene decorated by alkali metal adatoms (Li,K). *Appl. Phys. Lett.* **111**, 263502 (2017).
9. Uchoa, B. & Castro Neto, A. Superconducting States of Pure and Doped Graphene. *Phy. Rev. Lett.* **98**, 146801 (2007).
10. Nandkishore, R., Levitov, L. S. & Chubukov, A. V. Chiral superconductivity from repulsive interactions in doped graphene. *Nat. Phys.* **8**, 158–163 (2012).
11. Nandkishore, R., Thomale R. & Chubukov A. V. Superconductivity from weak repulsions in hexagonal lattice systems. *Phys. Rev. B* **89**, 144501 (2014).
12. Black-Schaffer, A. M. & Doniach, S. Resonating valence bonds and mean field d-wave superconductivity in graphene. *Phys. Rev. B* **75**, 134512 (2007).
13. Kiesel M. L. , Platt C., Hanke W. , Abanin D. A., & Thomale R. Competing many-body instabilities and unconventional superconductivity in graphene. *Phys. Rev. B* **86**, 020507R (2012).
14. Ma, T., Yang, F., Yao, H. & Lin H. Q. Possible triplet $p + ip$ superconductivity in graphene at low filling. *Phys. Rev. B* **90**, 245114 (2014).
15. Profeta, G., Calandra, M. & Mauri, F. Phonon-mediated superconductivity in graphene by Lithium deposition. *Nat. Phys.* **8**, 131-134 (2012).
16. Wong, C. H., Lortz, R., Buntov, E. A., Kasimova, R. E. & Zatsepin, A. F. A theoretical quest for high temperature superconductivity on the example of low-dimensional carbon structures. *Sci. Rep.* **7**, 15805 (2017).

17. Hou C. Y., Chamon, C., & Mudry C. Electron Fractionalization in Two-Dimensional Graphenelike Structures. Phys. Rev. Lett. **98**, 186809 (2007).
18. Wu, L. -H. & Hu, X. Topological Properties of Electrons in Honeycomb Lattice with Detuned Hopping Energy. Sci. Rep. **6**, 24347 (2016).
19. Guzman, D. M., Alyahyaei H. M. & Jishi, R. A. Superconductivity in graphene-lithium. 2D Materials **1**, (2014) 021005.
20. Wallace, P. R. The Band Theory of Graphite. Phys. Rev. **71**, 622 (1947).
21. Reich, S., Maultzsch, J., Thomsen, C. & Ordejón, P. Tight-binding description of graphene. Phys. Rev. B **66**, 035412 (2002).
22. Kundu, R. Tight Binding Parameters for Graphene. Mod. Phys. Lett. B **25**, 163 (2011).
23. Jung J. & MacDonald, A. H. Tight-binding model for graphene π -bands from maximally localized Wannier functions. Phys.Rev. B **87**, 195450 (2013).
24. Zheng, J. -J. & Margine, E. R. First-principles calculations of the superconducting properties in Li-decorated monolayer graphene within the anisotropic Migdal-Eliashberg formalism. Phys.Rev. B **94**, 064509 (2016).

Acknowledgments

R. Gholami acknowledges support that allowed an extended visit to the University of California Davis during part of this work. W.E.P. was supported by NSF grant DMR-1207622.

Author contributions

R. M. proposed the idea. R. G. and R. M. did the analytical derivation. R. G. carried out the numerical calculations under supervision of R. M. and W. E. P. and S. M. performed the DFT calculations. All authors analyzed the results and wrote the article.

Additional information

Competing interests: The authors declare no competing interests.

Appendices

A Accurate Tight Binding Model for Lithium decorated Graphene

The Hamiltonian of non-interacting LiC₆ is

$$\hat{H}_N = - \sum_{i\alpha} \sum_{j\beta, \sigma} t_{i\alpha, j\beta}^{\sigma, \sigma} c_{i\alpha\sigma}^\dagger c_{j\beta\sigma} + \sum_{i\alpha, \sigma} (\epsilon_{i\alpha} - \mu_o) \hat{n}_{i\alpha\sigma}. \quad (22)$$

Eq 22 can be diagonalized in terms of Bloch eigenfunctions of the form

$$|\Psi_{\vec{k}}\rangle = \frac{1}{\sqrt{N}} \sum_{n=1}^N \sum_{\alpha=1}^7 \mathcal{C}_\alpha e^{i\vec{k} \cdot \vec{r}_{n\alpha}} |\phi_{n\alpha}\rangle \quad (23)$$

in which $\vec{r}_{n\alpha} = \vec{r}_n + \vec{d}_\alpha$ and \vec{r}_n is n th Bravais lattice site vector position and \vec{d}_α is vector position of the α -th subsite with respect to unit cell n . $|\phi_{n\alpha}\rangle = |\phi_{n\alpha}(\vec{r} - \vec{r}_n - \vec{d}_\alpha)\rangle$ is the atomic π electron ket of atom α of cell n . By inserting Eqs. 22 and 23 into $\hat{H}_N(\vec{k}) |\Psi_{\vec{k}}\rangle = E(\vec{k}) |\Psi_{\vec{k}}\rangle$, the equation for the coefficients becomes

$$\sum_{\beta=1}^7 \epsilon_{\alpha\beta}(\vec{k}) \mathcal{C}_\beta + (\epsilon_\alpha - \mu_o) \mathcal{C}_\alpha = E(\vec{k}) \mathcal{C}_\alpha \text{ where } \epsilon_{\alpha\beta}(\vec{k}) = -\frac{1}{N} \sum_{ij} t_{i\alpha, j\beta}^{\sigma\sigma} e^{i\vec{k} \cdot (\vec{r}_{i\alpha} - \vec{r}_{j\beta})}. \quad (24)$$

Eq. 24 can be expressed in following matrix form

$$\left(\begin{array}{c|cc} \epsilon_{LiLi}(\vec{k}) + \epsilon_{Li} - \mu_o & h_{LiA}(\vec{k}) & h_{LiB}(\vec{k}) \\ \hline h_{LiA}^\dagger(\vec{k}) & h_{AA}(\vec{k}) + \epsilon_A - \mu_o & h_{AB}(\vec{k}) \\ h_{LiB}^\dagger(\vec{k}) & h_{BA}(\vec{k}) & h_{BB}(\vec{k}) + \epsilon_B - \mu_o \end{array} \right) \begin{pmatrix} \mathcal{C}_{Li}(E_i(\vec{k})) \\ \xi_A(E_i(\vec{k})) \\ \xi_B(E_i(\vec{k})) \end{pmatrix} = E_i(\vec{k}) \begin{pmatrix} \mathcal{C}_{Li}(E_i(\vec{k})) \\ \xi_A(E_i(\vec{k})) \\ \xi_B(E_i(\vec{k})) \end{pmatrix} \quad (25)$$

where

$$\begin{aligned}\varepsilon_{LiLi}(\vec{k}) &= 2t_1^{LiLi} \left(\cos \vec{k} \cdot \vec{\xi}_1 + \cos \vec{k} \cdot \vec{\xi}_2 + \cos \vec{k} \cdot \vec{\xi}_3 \right) + 2t_2^{LiLi} \left(\cos \vec{k} \cdot (\vec{\xi}_1 - \vec{\xi}_2) + \cos \vec{k} \cdot (\vec{\xi}_1 - \vec{\xi}_3) + \cos \vec{k} \cdot (\vec{\xi}_2 - \vec{\xi}_3) \right) \\ &+ 2t_3^{LiLi} \left(\cos 2\vec{k} \cdot \vec{\xi}_1 + \cos 2\vec{k} \cdot \vec{\xi}_2 + \cos 2\vec{k} \cdot \vec{\xi}_3 \right) + \dots\end{aligned}\quad (26)$$

In Eq. 25, h -sub-block matrices are C-C or Li-C dispersion matrices and we have $h_{AA} = h_{BB}^*$, $h_{AB} = h_{BA}^\dagger$. The carbon-carbon dispersion matrices i.e. $\varepsilon_{(A,B)_i(A,B)_j}(\vec{k})$ are

$$h_{AA}(\vec{k}) = \begin{pmatrix} \alpha(\vec{k}) & \beta(\vec{k}) & \gamma(\vec{k}) \\ \beta^*(\vec{k}) & \alpha(\vec{k}) & \theta(\vec{k}) \\ \gamma^*(\vec{k}) & \theta^*(\vec{k}) & \alpha(\vec{k}) \end{pmatrix}, \quad h_{AB}(\vec{k}) = \begin{pmatrix} \tau_1(\vec{k}) & d_2(\vec{k}) & d_3(\vec{k}) \\ d_2(\vec{k}) & \tau_3(\vec{k}) & d_1(\vec{k}) \\ d_3(\vec{k}) & d_1(\vec{k}) & \tau_2(\vec{k}) \end{pmatrix}\quad (27)$$

The Li-C dispersion row matrices i.e. $\varepsilon_{LiA_i}(\vec{k})$ and $\varepsilon_{LiB_i}(\vec{k})$ are

$$h_{LiA}(\vec{k}) = [d_{1c}(\vec{k}) \ d_{3c}(\vec{k}) \ d_{2c}(\vec{k})] = -t_1^{LiC} e^{ik_z h} \begin{pmatrix} e^{i\vec{k} \cdot \vec{\delta}_1} & e^{i\vec{k} \cdot \vec{\delta}_3} & e^{i\vec{k} \cdot \vec{\delta}_2} \end{pmatrix}, \quad h_{LiB}(\vec{k}) = e^{ik_z h} h_{LiA}^*(\vec{k})\quad (28)$$

where $e^{k_z h}$ factor takes 1 by confinement. New variables, \vec{k} dependent on-site energy and chemical potential has been defined as

$$\begin{aligned}\varepsilon_0(\vec{k}) &= \varepsilon_{Li} - \mu_o + \varepsilon_{LiLi}(\vec{k}) \\ \varepsilon_1(\vec{k}) &= \varepsilon_A - \mu_o + \varepsilon_{A_1A_1}(\vec{k}) \\ \varepsilon_2(\vec{k}) &= \varepsilon_B - \mu_o + \varepsilon_{B_1B_1}(\vec{k})\end{aligned}\quad (29)$$

Shorthand notation has been introduced as follows,

$$\begin{aligned}\alpha(\vec{k}) \equiv \varepsilon_{A_iA_i}(\vec{k}) &= \varepsilon_{B_iB_i}(\vec{k}) = -t_0 - 2t_5 \left(\cos \vec{k} \cdot \vec{\xi}_1 + \cos \vec{k} \cdot \vec{\xi}_2 + \cos \vec{k} \cdot \vec{\xi}_3 \right) \\ \beta(\vec{k}) \equiv \varepsilon_{A_1A_2}(\vec{k}) &= \varepsilon_{A_2A_1}^*(\vec{k}) = -t_2 e^{i\vec{k} \cdot (\vec{\delta}_3 - \vec{\delta}_1)} \left[1 + w_t \left(e^{-i\vec{k} \cdot \vec{\xi}_3} + e^{i\vec{k} \cdot \vec{\xi}_1} \right) \right] \\ \gamma(\vec{k}) \equiv \varepsilon_{A_1A_3}(\vec{k}) &= \varepsilon_{A_3A_1}^*(\vec{k}) = -t_2 e^{i\vec{k} \cdot (\vec{\delta}_2 - \vec{\delta}_1)} \left[1 + w_t \left(e^{-i\vec{k} \cdot \vec{\xi}_2} + e^{i\vec{k} \cdot \vec{\xi}_1} \right) \right] \\ \theta(\vec{k}) \equiv \varepsilon_{A_2A_3}(\vec{k}) &= \varepsilon_{A_3A_2}^*(\vec{k}) = -t_2 e^{i\vec{k} \cdot (\vec{\delta}_2 - \vec{\delta}_3)} \left[1 + w_t \left(e^{-i\vec{k} \cdot \vec{\xi}_2} + e^{i\vec{k} \cdot \vec{\xi}_3} \right) \right]\end{aligned}\quad (30)$$

in which $w_t = \frac{t'_1}{t_1} = \frac{t'_2}{t_2}$ and $\vec{\xi}_i = \vec{\tau}_i + 2\vec{\delta}_i$ the d and τ functions are given by

$$\begin{aligned}\tau_1(\vec{k}) &= -t'_1 e^{i\vec{k} \cdot \vec{\tau}_1} \left[1 + \frac{t_3}{t_1} e^{-i\vec{k} \cdot \vec{\xi}_1} + \frac{t_4}{t_1} \left(e^{i\vec{k} \cdot \vec{\xi}_2} + e^{i\vec{k} \cdot \vec{\xi}_3} \right) \right], \quad d_1(\vec{k}) = -t_1 e^{i\vec{k} \cdot \vec{\delta}_1} \left[1 + \frac{t_3}{t_1} e^{-i\vec{k} \cdot \vec{\xi}_1} + \frac{t_4}{t_1} \left(e^{i\vec{k} \cdot \vec{\xi}_2} + e^{i\vec{k} \cdot \vec{\xi}_3} \right) \right] \\ \tau_2(\vec{k}) &= -t'_1 e^{i\vec{k} \cdot \vec{\tau}_2} \left[1 + \frac{t_3}{t_1} e^{-i\vec{k} \cdot \vec{\xi}_2} + \frac{t_4}{t_1} \left(e^{i\vec{k} \cdot \vec{\xi}_3} + e^{i\vec{k} \cdot \vec{\xi}_1} \right) \right], \quad d_2(\vec{k}) = -t_1 e^{i\vec{k} \cdot \vec{\delta}_2} \left[1 + \frac{t_3}{t_1} e^{-i\vec{k} \cdot \vec{\xi}_2} + \frac{t_4}{t_1} \left(e^{i\vec{k} \cdot \vec{\xi}_3} + e^{i\vec{k} \cdot \vec{\xi}_1} \right) \right] \\ \tau_3(\vec{k}) &= -t'_1 e^{i\vec{k} \cdot \vec{\tau}_3} \left[1 + \frac{t_3}{t_1} e^{-i\vec{k} \cdot \vec{\xi}_3} + \frac{t_4}{t_1} \left(e^{i\vec{k} \cdot \vec{\xi}_1} + e^{i\vec{k} \cdot \vec{\xi}_2} \right) \right], \quad d_3(\vec{k}) = -t_1 e^{i\vec{k} \cdot \vec{\delta}_3} \left[1 + \frac{t_3}{t_1} e^{-i\vec{k} \cdot \vec{\xi}_3} + \frac{t_4}{t_1} \left(e^{i\vec{k} \cdot \vec{\xi}_1} + e^{i\vec{k} \cdot \vec{\xi}_2} \right) \right].\end{aligned}\quad (31)$$

Also

$$\xi_A(\vec{k}) = \begin{pmatrix} \mathcal{C}_{A_1}(E_i(\vec{k})) \\ \mathcal{C}_{A_2}(E_i(\vec{k})) \\ \mathcal{C}_{A_3}(E_i(\vec{k})) \end{pmatrix}; \quad \xi_B(\vec{k}) = \begin{pmatrix} \mathcal{C}_{B_1}(E_i(\vec{k})) \\ \mathcal{C}_{B_2}(E_i(\vec{k})) \\ \mathcal{C}_{B_3}(E_i(\vec{k})) \end{pmatrix}.\quad (32)$$

Since the Li is an inversion center of the two-dimension tight binding model, the Bloch wave function should respect inversion symmetry. Using $\Psi_{\vec{k}}(\vec{r}) = \langle \vec{r} | \Psi_{\vec{k}} \rangle$, the condition is

$$\Psi_{-\vec{k}}(-\vec{r}) = C e^{i\phi} \Psi_{\vec{k}}(\vec{r}),\quad (33)$$

where C is ± 1 when all subsites in hexagons are carbon, that is $\varepsilon_{A_i} = \varepsilon_{B_i}$. This condition is satisfied if \mathcal{C}_{A_i} is proportional to $\mathcal{C}_{B_i}^*$

$$\mathcal{C}_{A_m}(E_i(\vec{k})) = f_i(\vec{k}) \mathcal{C}_{B_m}^*(E_i(\vec{k})), \quad \text{and} \quad \mathcal{C}_{Li}(E_i(\vec{k})) = f_i(\vec{k}) \mathcal{C}_{Li}^*(E_i(\vec{k})), \quad i = 1, 2, \dots, 7\quad (34)$$

where $f_i(\vec{k})$ is a coefficient to be determined. By inserting $\mathcal{C}_{A_i} = |\mathcal{C}_{A_i}|e^{i\phi_{A_i}}$ and $\mathcal{C}_{B_i} = |\mathcal{C}_{B_i}|e^{i\phi_{B_i}}$ into Eq. 34 we have

$$f_i(\vec{k}) = \frac{|\mathcal{C}_{A_m}(E_i(\vec{k}))|}{|\mathcal{C}_{B_m}(E_i(\vec{k}))|} e^{i(\phi_{A_i} + \phi_{B_i})} = C_i e^{i\phi_i}, \quad i = 1, 2, \dots, 7. \quad (35)$$

In the next subsection we use Eqs. 34 and 35 to reduce the eigenvalue Eq. 24 in matrix form to 3×3 to obtain uncoupled shrunken graphene band structure and Bloch wave function coefficients.

B Uncoupled C_6 Dispersion Relations

By first neglecting the lithium-carbon hopping $t_1^{LiC} \rightarrow 0$, the shrunken graphene Hamiltonian Eq. 25 can be diagonalized exactly. Our notation is

$$\begin{pmatrix} \varepsilon_0(\vec{k}) & 0 & 0 & 0 & 0 & 0 & 0 \\ 0 & \varepsilon_1(\vec{k}) & \beta(\vec{k}) & \gamma(\vec{k}) & \tau_1(\vec{k}) & d_2(\vec{k}) & d_3(\vec{k}) \\ 0 & \beta^*(\vec{k}) & \varepsilon_1(\vec{k}) & \theta(\vec{k}) & d_2(\vec{k}) & \tau_3(\vec{k}) & d_1(\vec{k}) \\ 0 & \gamma^*(\vec{k}) & \theta^*(\vec{k}) & \varepsilon_1(\vec{k}) & d_3(\vec{k}) & d_1(\vec{k}) & \tau_2(\vec{k}) \\ 0 & \tau_1^*(\vec{k}) & d_2^*(\vec{k}) & d_3^*(\vec{k}) & \varepsilon_2(\vec{k}) & \beta^*(\vec{k}) & \gamma^*(\vec{k}) \\ 0 & d_2^*(\vec{k}) & \tau_3^*(\vec{k}) & d_1^*(\vec{k}) & \beta(\vec{k}) & \varepsilon_2(\vec{k}) & \theta^*(\vec{k}) \\ 0 & d_3^*(\vec{k}) & d_1^*(\vec{k}) & \tau_2^*(\vec{k}) & \gamma(\vec{k}) & \theta(\vec{k}) & \varepsilon_2(\vec{k}) \end{pmatrix} \begin{pmatrix} C_{Li}(E_i^0(\vec{k})) \\ C_{A_1}(E_i^0(\vec{k})) \\ C_{A_2}(E_i^0(\vec{k})) \\ C_{A_3}(E_i^0(\vec{k})) \\ C_{B_1}(E_i^0(\vec{k})) \\ C_{B_2}(E_i^0(\vec{k})) \\ C_{B_3}(E_i^0(\vec{k})) \end{pmatrix} = E_i^0(\vec{k}) \begin{pmatrix} C_{Li}(E_i^0(\vec{k})) \\ C_{A_1}(E_i^0(\vec{k})) \\ C_{A_2}(E_i^0(\vec{k})) \\ C_{A_3}(E_i^0(\vec{k})) \\ C_{B_1}(E_i^0(\vec{k})) \\ C_{B_2}(E_i^0(\vec{k})) \\ C_{B_3}(E_i^0(\vec{k})) \end{pmatrix} \quad (36)$$

The non trivial eigenvalues of uncoupled Hamiltonian Eq. 36 are given by

$$E_{sh,n}(\vec{k}) = E_{sh,ml}(t_i, \vec{\xi}_i, \vec{k}) = -\mu_o + \alpha(\vec{k}) + u_m \Pi_0(\vec{k}) + u_m^* \Pi_0^*(\vec{k}) + \frac{1}{2} \left[\varepsilon_A + \varepsilon_B + (-1)^l \sqrt{(\varepsilon_A - \varepsilon_B)^2 + 4w_m(\vec{k})} \right] \quad (37)$$

where n is band index defined as

$$n = (2l+1) + (-1)^l m; \quad m = \begin{cases} 0, 1, 2 & \text{for } l=0 \text{ conduction} \\ -1, -2, -3 & \text{for } l=1 \text{ valence} \end{cases} \quad (38)$$

Here $E_{sh,1}$, $E_{sh,2}$ and $E_{sh,3}$ are conduction bands which corresponds to $l = 0$ and $m = 0, 1, 2$ and $E_{sh,4}$, $E_{sh,5}$ and $E_{sh,6}$ are valence bands which correspond to $l = 1$, $m = -1, -2, -3$.

At the Γ point, when $\varepsilon_A = \varepsilon_B = \varepsilon^c$, the shrunk graphene eigenstates $|\phi_n(0)\rangle = (C_{A_1} \ C_{A_2} \ C_{A_3} \ C_{B_1} \ C_{B_2} \ C_{B_3})^T$ over the hexagonal subsites take the forms similar to conventional s , d and p orbitals,

$$\begin{aligned} |f\rangle &= (1 \ 1 \ 1 \ -1 \ -1 \ -1)^T, \quad |p_x\rangle = (1 \ -1 \ 0 \ -1 \ 1 \ 0)^T, \quad |p_y\rangle = (1 \ 1 \ -2 \ -1 \ -1 \ 2)^T, \\ |d_{x^2-y^2}\rangle &= (1 \ 1 \ -2 \ 1 \ 1 \ -2)^T, \quad |d_{xy}\rangle = (1 \ -1 \ 0 \ 1 \ -1 \ 0)^T, \quad |S\rangle = (1 \ 1 \ 1 \ 1 \ 1 \ 1)^T, \end{aligned} \quad (39)$$

with energies,

$$\begin{aligned} E_f &= E_\gamma^+(0) = \mu_s + [(t_1' + 2t_1) + 3t_3 + 6t_4] \\ E_s &= E_\gamma^-(0) = \mu_s - [(t_1' + 2t_1) + 3t_3 + 6t_4] \\ E_p &= E_\alpha^+(0) = E_\beta^+(0) = \mu_d + (t_1' - t_1) \\ E_d &= E_\alpha^-(0) = E_\beta^-(0) = \mu_d - (t_1' - t_1) \end{aligned} \quad (40)$$

where $\mu_s = \varepsilon^c - \mu_0 - 2(t_2 + 2t_2') - 6t_5$ and $\mu_d = \varepsilon^c - \mu_0 + (t_2 + 2t_2') - 6t_5$. For general \vec{k} the uncoupled shrunken graphene eigenfunction Eq. 59 can be written in terms of $|S\rangle$, $|f\rangle$, $|p_x\rangle$, $|p_y\rangle$, $|d_{xy}\rangle$ and $|d_{x^2-y^2}\rangle$ as

$$|\phi_n(\vec{k})\rangle = (f_s^n(\vec{k})|S\rangle + f_f^n(\vec{k})|f\rangle) + (f_{p_y}^n(\vec{k})|p_y\rangle + i f_{d_{xy}}^n(\vec{k})|d_{xy}\rangle) + (f_{d_{x^2-y^2}}^n(\vec{k})|d_{x^2-y^2}\rangle + i f_{p_x}^n(\vec{k})|p_x\rangle). \quad (41)$$

In the particular case of pristine graphene in which $w_t = 1$ and $\vec{\tau}_1 = \vec{\delta}_1$, $\vec{\tau}_2 = \vec{\delta}_2$, $\vec{\tau}_3 = \vec{\delta}_3$, hence $\beta = \theta = \gamma^*$ and also $\varepsilon_A = \varepsilon_B$ so $C = \pm 1$. Therefore eigenvectors take following form

$$|\phi_{m,l}^0(\vec{k})\rangle = \frac{1}{\sqrt{6}} \left(\omega_m \ \omega_m^* \ 1 \ (-1)^l \frac{\eta_m^*}{|\eta_m|} \omega_m^* \ (-1)^l \frac{\eta_m^*}{|\eta_m|} \omega_m \ (-1)^l \frac{\eta_m^*}{|\eta_m|} \right)^T, \quad \omega_m = e^{i2\pi m/3}, \quad (42)$$

where $m = 1, 2, 3$; $l = 0, 1$ and $\eta_m(\vec{k}) = d_2(\vec{k}) + \omega_m d_1(\vec{k}) + \omega_m^* d_3(\vec{k})$. The eigenvalues are

$$E_{m,l}^0 = \varepsilon_{A_1 A_1}(\vec{k}) + \omega_m \beta(\vec{k}) + \omega_m^* \beta^*(\vec{k}) + (-1)^l t_1 |\eta_m(\vec{k})| \quad (43)$$

By comparing pristine eigenvectors Eq. 42 with general shrunken graphene eigenvectors Eq. 41 it is found that for $m = 1$, $f_{d_{x^2-y^2}}^1(\vec{k}) = -f_{p_x}^1(\vec{k}) = \frac{(1-e^{i\phi_1})}{2\sqrt{2}}$ which corresponds to $d_{x^2-y^2} - ip_x$, also $f_{p_y}^1(\vec{k}) = -f_{d_{xy}}^1(\vec{k}) = \frac{(1+e^{i\phi_1})}{2\sqrt{2}}$ which corresponds to $p_y - id_{xy}$, and the coefficients of s and f are zero. For $m = 2$, $f_{d_{x^2-y^2}}^2(\vec{k}) = f_{p_x}^2(\vec{k}) = \frac{(1-e^{i\phi_2})}{2\sqrt{2}}$ which corresponds to $d_{x^2-y^2} + ip_x$ also $f_{p_y}^2(\vec{k}) = f_{d_{xy}}^2(\vec{k}) = \frac{(1+e^{i\phi_2})}{2\sqrt{2}}$ which corresponds to $p_y + id_{xy}$ while s and f coefficients are zero. For $m = 3$, $f_s^3(\vec{k}) = \frac{(1-e^{i\phi_3})}{2}$ and $f_f^3(\vec{k}) = \frac{(1+e^{i\phi_3})}{2}$ and other coefficients are zero. Here, $e^{i\phi_m} = \frac{\eta_m^*}{|\eta_m|}$.

The Hamiltonian \hat{H}_N^{shr} for the broken symmetry (shrunk graphene) is 6×6 in terms of 3×3 subblocks

$$\begin{pmatrix} h_{AA}(\vec{k}) + \varepsilon_A - \mu_o & h_{AB}(\vec{k}) \\ h_{BA}(\vec{k}) & h_{AA}^*(\vec{k}) + \varepsilon_B - \mu_o \end{pmatrix} \begin{pmatrix} \xi_A^0(E_{sh;i}(\vec{k})) \\ \xi_B^0(E_{sh;i}(\vec{k})) \end{pmatrix} = E_{sh;i}(\vec{k}) \begin{pmatrix} \xi_A^0(E_{sh;i}(\vec{k})) \\ \xi_B^0(E_{sh;i}(\vec{k})) \end{pmatrix} \quad (44)$$

To solve Schrödinger Eq. 44 we first separate the left hand side of Eq. 44 into two terms $H_{sh}(\vec{k}) = H_{sh}^0(\vec{k}) + H_{sh}^1(\vec{k})$ where

$$H_{sh}^0(\vec{k}) = \begin{pmatrix} \varepsilon_1(\vec{k}) I_{3 \times 3} & h_{AB}(\vec{k}) \\ h_{BA}(\vec{k}) & \varepsilon_2(\vec{k}) I_{3 \times 3} \end{pmatrix}, \quad H_{sh}^1(\vec{k}) = \begin{pmatrix} h'_{aa}(\vec{k}) & 0_{3 \times 3} \\ 0_{3 \times 3} & h'_{bb}(\vec{k}) \end{pmatrix} \quad (45)$$

where $h'_{aa}(\vec{k}) = (h_{AA}(\vec{k}) - \alpha(\vec{k}) I_{3 \times 3})$. In the nearest neighbor approximation it is straightforward to show that $H_{sh}^0(\vec{k})$ and $H_{sh}^1(\vec{k})$ commute with each other, hence they have the same eigenvectors. In more generality one can consider approximately the eigenvectors of H_{sh}^1 to be the same as the eigenvectors of H_{sh}^0 , therefore one obtains

$$\xi_B^0(\vec{k}) = C e^{i\phi} \xi_A^{0*} : \quad E_{sh}(\vec{k}) \approx E_{sh}^0(\vec{k}) + E_{sh}^1(\vec{k}). \quad (46)$$

with the first equation arising from similar conditions as for Eq. 34. To find $E_{sh}(\vec{k})$ we solve the following eigenvalue problems

$$\begin{pmatrix} h'_{aa}(\vec{k}) & 0_{3 \times 3} \\ 0_{3 \times 3} & h'_{aa}^*(\vec{k}) \end{pmatrix} \begin{pmatrix} \xi_A^0(\vec{k}) \\ \xi_B^0(\vec{k}) \end{pmatrix} = E_{sh}^1(\vec{k}) \begin{pmatrix} \xi_A^0(\vec{k}) \\ \xi_B^0(\vec{k}) \end{pmatrix} \quad (47)$$

and

$$\begin{pmatrix} \varepsilon_1(\vec{k}) I_{3 \times 3} & h_{AB}(\vec{k}) \\ h_{BA}(\vec{k}) & \varepsilon_2(\vec{k}) I_{3 \times 3} \end{pmatrix} \begin{pmatrix} \xi_A^0(\vec{k}) \\ \xi_B^0(\vec{k}) \end{pmatrix} = E_{sh}^0(\vec{k}) \begin{pmatrix} \xi_A^0(\vec{k}) \\ \xi_B^0(\vec{k}) \end{pmatrix} \quad (48)$$

Eq. 47 converts to following eigenvalue problem $h'_{aa}(\vec{k}) \xi_A^0(\vec{k}) = E_{sh}^1(\vec{k}) \xi_A^0(\vec{k})$ and its complex conjugate with $A \leftrightarrow B$, defining

$$\begin{aligned} c_0(t_2, \vec{\xi}_i, \vec{k}) &= \beta(\vec{k}) \theta(\vec{k}) \gamma^*(\vec{k}) + \gamma(\vec{k}) \beta^*(\vec{k}) \theta^*(\vec{k}), \quad c_1(t_2, \vec{\xi}_i, \vec{k}) = |\beta(\vec{k})|^2 + |\theta(\vec{k})|^2 + |\gamma(\vec{k})|^2 \\ \Pi_0(t_2, \vec{\xi}_i, \vec{k}) &= \left(\frac{c_0(t_2, \vec{\xi}_i, \vec{k})}{2} + i \sqrt{\left(\frac{c_1(t_2, \vec{\xi}_i, \vec{k})}{3} \right)^3 - \left(\frac{c_0(t_2, \vec{\xi}_i, \vec{k})}{2} \right)^2} \right)^{1/3}. \end{aligned} \quad (49)$$

eigenvalue equation Eq. 47 has the three different eigenvalues

$$E_{sh,m}^1(t_2, \vec{\xi}_i, \vec{k}) = u_m \Pi_0(t_2, \vec{\xi}_i, \vec{k}) + u_m^* \Pi_0^*(t_2, \vec{\xi}_i, \vec{k}); \quad u_m = \sqrt[3]{1} = e^{4im\pi/3}; \quad m = 1, 2, 3 \quad (50)$$

note that $E_{sh,m}^1(t_2, \vec{\xi}_i, \vec{k})$ is function of second neighbor hopping $t_{<iA_i, jA_j>} = t_2$ and $\vec{\xi}_i = \vec{r}_i + 2\vec{\delta}_i$ i.e. lattice bases vector and it does not depend on \vec{r}_i and $\vec{\delta}_i$ separately. Now we calculate $E_{sh}^0(\vec{k})$. Eq. 48 can be separated into following equations

$$h_{AB}(\vec{k}) \xi_B^0(\vec{k}) = (E_{sh}^0(\vec{k}) - \varepsilon_1(\vec{k})) \xi_A^0(\vec{k}), \quad h_{BA}(\vec{k}) \xi_A^0(\vec{k}) = (E_{sh}^0(\vec{k}) - \varepsilon_2(\vec{k})) \xi_B^0(\vec{k}). \quad (51)$$

By multiplying first equation of Eq. 51 by h_{BA} and second by h_{AB} we have

$$\begin{aligned} h_{AB}(\vec{k}) h_{BA}(\vec{k}) \xi_A^0(\vec{k}) &= (E_{sh}^0(\vec{k}) - \varepsilon_1(\vec{k})) (E_{sh}^0(\vec{k}) - \varepsilon_2(\vec{k})) \xi_A^0(\vec{k}) \\ h_{BA}(\vec{k}) h_{AB}(\vec{k}) \xi_B^0(\vec{k}) &= (E_{sh}^0(\vec{k}) - \varepsilon_1(\vec{k})) (E_{sh}^0(\vec{k}) - \varepsilon_2(\vec{k})) \xi_B^0(\vec{k}). \end{aligned} \quad (52)$$

Eq. 52 is an eigenvalue problem where second equation is just complex conjugated of first one. By defining new matrix $G(\vec{k}) = h_{AB}(\vec{k})h_{BA}(\vec{k})$ and $w_i(\vec{k}) = [E_{sh,i}^0(\vec{k})]^2 - [\epsilon_1(\vec{k}) + \epsilon_2(\vec{k})]E_{sh,i}^0(\vec{k}) + \epsilon_1(\vec{k})\epsilon_2(\vec{k})$, Eq. 52 takes the form

$$G(\vec{k})\xi_A^0(E_i^0(\vec{k})) = w_i(\vec{k})\xi_A^0(E_i^0(\vec{k})) \quad (53)$$

Schrödinger Eq. 53 can be solved to find eigenvalues of Eq. 48 i.e. $E_{sh}^0(\vec{k})$. Defining

$$\begin{aligned} C_2(t_i, \vec{\xi}_i, \vec{k}) &= G_{11} + G_{22} + G_{33} \\ C_1(t_i, \vec{\xi}_i, \vec{k}) &= |G_{12}|^2 + |G_{13}|^2 + |G_{23}|^2 - (G_{11}G_{22} + G_{11}G_{33} + G_{22}G_{33}) \\ C_0(t_i, \vec{\xi}_i, \vec{k}) &= G_{13}(G_{12}G_{23})^* + G_{13}^*(G_{12}G_{23}) - G_{11}|G_{23}|^2 - G_{22}|G_{13}|^2 - G_{33}|G_{12}|^2 + G_{11}G_{22}G_{33} \end{aligned} \quad (54)$$

where $G_{ij} = \sum_{m=1}^3 \epsilon_{A_i B_m}(\vec{k})\epsilon_{B_m A_j}(\vec{k})$. Also introducing

$$\begin{aligned} \Pi_1(t_i, \vec{\xi}_i, \vec{k}) &= \left(Q(t_i, \vec{\xi}_i, \vec{k}) + i\sqrt{P(t_i, \vec{\xi}_i, \vec{k})^3 - Q(t_i, \vec{\xi}_i, \vec{k})^2} \right)^{\frac{1}{3}} \\ Q(t_i, \vec{\xi}_i, \vec{k}) &= \frac{C_0(t_i, \vec{\xi}_i, \vec{k})}{2} + \frac{C_1(t_i, \vec{\xi}_i, \vec{k})C_2(t_i, \vec{\xi}_i, \vec{k})}{6} + \frac{C_2^3(t_i, \vec{\xi}_i, \vec{k})}{27} \\ P(t_i, \vec{\xi}_i, \vec{k}) &= \frac{C_1(t_i, \vec{\xi}_i, \vec{k})}{3} + \frac{C_2^2(t_i, \vec{\xi}_i, \vec{k})}{9}. \end{aligned} \quad (55)$$

where $t_i = t_{iA_jB}$ are first, 3rd and 4th neighbor hopping integrals. Hence eigenvalues of Eq. 48 can be obtained, they are

$$E_{sh;m,l}^0(t_i, \vec{\xi}_i, \vec{k}) = \epsilon_{A_1 A_1}(\vec{k}) - \mu_o + \frac{1}{2} \left[\epsilon_A + \epsilon_B + (-1)^l \sqrt{(\epsilon_A - \epsilon_B)^2 + 4w_m(t_i, \vec{\xi}_i, \vec{k})} \right] \quad (56)$$

where $l = 0, 1$ and $w_m(t_i, \vec{\xi}_i, \vec{k})$ i.e. solutions of Schrödinger Eq. 53 are

$$w_m(t_i, \vec{\xi}_i, \vec{k}) = \frac{C_2(t_i, \vec{\xi}_i, \vec{k})}{3} + u_m \Pi_1(t_i, \vec{\xi}_i, \vec{k}) + u_m^* \Pi_1^*(t_i, \vec{\xi}_i, \vec{k}) \quad ; u_m = \sqrt[3]{1} = e^{4im\pi/3} \quad ; m = 1, 2, 3. \quad (57)$$

Hence from Eqs. 46, 50 and 56 eigenvalues of Schrödinger Eq. 44 can be obtained,

$$E_{sh;m,l}(t_i, \vec{\xi}_i, \vec{k}) = E_{sh,m}^1(t_i, \vec{\xi}_i, \vec{k}) + \epsilon_{A_1 A_1}(\vec{k}) - \mu_o + \frac{1}{2} \left[\epsilon_A + \epsilon_B + (-1)^l \sqrt{(\epsilon_A - \epsilon_B)^2 + 4w_m(t_i, \vec{\xi}_i, \vec{k})} \right] \quad (58)$$

The corresponding orthogonal eigenvectors are

$$\left| \phi(E_{sh,n}(\vec{k})) \right\rangle = C_{A_3}(E_{sh,n}(\vec{k})) \left[\begin{pmatrix} \frac{C_{A_1}(E_{sh,n}(\vec{k}))}{C_{A_3}(E_{sh,n}(\vec{k}))} & \frac{C_{A_2}(E_{sh,n}(\vec{k}))}{C_{A_3}(E_{sh,n}(\vec{k}))} & 1 \end{pmatrix} C \frac{\eta^*(E_{sh,n}(\vec{k}))}{|\eta(E_{sh,n}(\vec{k}))|} \begin{pmatrix} \frac{C_{A_1}^*(E_{sh,n}(\vec{k}))}{C_{A_3}^*(E_{sh,n}(\vec{k}))} & \frac{C_{A_2}^*(E_{sh,n}(\vec{k}))}{C_{A_3}^*(E_{sh,n}(\vec{k}))} & 1 \end{pmatrix} \right]^T \quad (59)$$

where $C_{A_3}(E_{sh,n}(\vec{k}))$ can be found from orthogonality condition. Also,

$$\begin{aligned} C_{A_1}(E_{sh,i}(\vec{k})) &= \frac{-\left(G_{22} - w_i(\vec{k})\right)G_{13} + G_{12}G_{23}}{\left(G_{11} - w_i(\vec{k})\right)\left(G_{22} - w_i(\vec{k})\right) - |G_{12}|^2} C_{A_3}(E_{sh,i}(\vec{k})) \\ C_{A_2}(E_{sh,i}(\vec{k})) &= \frac{-\left(G_{11} - w_i(\vec{k})\right)G_{23} + G_{21}G_{13}}{\left(G_{11} - w_i(\vec{k})\right)\left(G_{22} - w_i(\vec{k})\right) - |G_{12}|^2} C_{A_3}(E_{sh,i}(\vec{k})). \end{aligned} \quad (60)$$

To find $\xi_B(E_n^0(\vec{k}))$ it has been used symmetry condition in Eq. 46

$$C_{B_m}(E_{sh,i}(\vec{k})) = C e^{i\varphi(E_{sh,i}(\vec{k}))} C_{A_m}^*(E_{sh,i}(\vec{k})). \quad (61)$$

Replacing Eq. 61 into second equation of Eq. 51 we get

$$\begin{aligned} e^{i\varphi(E_{sh,i}(\vec{k}))} &= \frac{\eta^*(E_{sh,i}(\vec{k}))}{|\eta(E_{sh,i}(\vec{k}))|} \frac{C_{A_3}(E_{sh,i}(\vec{k}))}{C_{A_3}^*(E_{sh,i}(\vec{k}))} \quad ; \quad C = \frac{E_{sh,i}^0(\vec{k}) - \epsilon_1(\vec{k})}{E_{sh,i}^0(\vec{k}) - \epsilon_2(\vec{k})} \\ \eta(E_{sh,i}(\vec{k})) &= -t_1 \left(d_3 \frac{C_{A_1}^*(E_{sh,i}(\vec{k}))}{C_{A_3}^*(E_{sh,i}(\vec{k}))} + d_2 \frac{C_{A_2}^*(E_{sh,i}(\vec{k}))}{C_{A_3}^*(E_{sh,i}(\vec{k}))} + \tau_2 \right). \end{aligned} \quad (62)$$

It is easy to show that $|\eta(E_{sh,i}(\vec{k}))| = w_i(\vec{k})$

C Coupled Li-C₆ dispersion relations

By applying the following unitary transformation, $P_{0N}^\dagger \hat{H}_N P_{0N} (P_{0N}^\dagger |\Psi_{\vec{k},n}(\vec{r})\rangle) = E_n(\vec{k}) P_{0N}^\dagger |\Psi_{\vec{k},n}(\vec{r})\rangle$, where \hat{P}_{0N} is the operator that diagonalize Eq. 36, the Schrödinger Eq. 25 is written in a new matrix representation as

$$\begin{pmatrix} E_{Li,0}(\vec{k}) & \gamma_1(\vec{k}) & \gamma_2(\vec{k}) & \gamma_3(\vec{k}) & \gamma_4(\vec{k}) & \gamma_5(\vec{k}) & \gamma_6(\vec{k}) \\ \gamma_1^*(\vec{k}) & E_{sh,1}(\vec{k}) & 0 & 0 & 0 & 0 & 0 \\ \gamma_2^*(\vec{k}) & 0 & E_{sh,2}(\vec{k}) & 0 & 0 & 0 & 0 \\ \gamma_3^*(\vec{k}) & 0 & 0 & E_{sh,3}(\vec{k}) & 0 & 0 & 0 \\ \gamma_4^*(\vec{k}) & 0 & 0 & 0 & E_{sh,4}(\vec{k}) & 0 & 0 \\ \gamma_5^*(\vec{k}) & 0 & 0 & 0 & 0 & E_{sh,5}(\vec{k}) & 0 \\ \gamma_6^*(\vec{k}) & 0 & 0 & 0 & 0 & 0 & E_{sh,6}(\vec{k}) \end{pmatrix} \begin{pmatrix} A_0(E_i(\vec{k})) \\ A_1(E_i(\vec{k})) \\ A_2(E_i(\vec{k})) \\ A_3(E_i(\vec{k})) \\ A_4(E_i(\vec{k})) \\ A_5(E_i(\vec{k})) \\ A_6(E_i(\vec{k})) \end{pmatrix} = E_i(\vec{k}) \begin{pmatrix} A_0(E_i(\vec{k})) \\ A_1(E_i(\vec{k})) \\ A_2(E_i(\vec{k})) \\ A_3(E_i(\vec{k})) \\ A_4(E_i(\vec{k})) \\ A_5(E_i(\vec{k})) \\ A_6(E_i(\vec{k})) \end{pmatrix} \quad (63)$$

where the relation between the column matrix eigenstate of Eq. 63, $A(E_i(\vec{k}))$, and the eigenstates of Eq. 25, \mathcal{C} is

$$A = P_{0N}^\dagger \mathcal{C}, \text{ and } A_j(E_i(\vec{k})) = \frac{\gamma_j^*}{E_i(\vec{k}) - E_{sh,j}(\vec{k})} A_0(E_i(\vec{k})) \quad (64)$$

in which $A_0(E_i(\vec{k}))$ is determined from the normalization condition, and also

$$\gamma_i(\vec{k}) = -t_1^{LiC} \sum_{m=1}^3 (C_{A_m}(E_{sh,i}(\vec{k})) e^{i\vec{k} \cdot \vec{\zeta}_{A_m}} + C_{B_m}(E_{sh,i}(\vec{k})) e^{i\vec{k} \cdot \vec{\zeta}_{B_m}}) \quad (65)$$

where $\vec{\zeta}_{A_m}$ is a vector that connects Li to the A_m carbon atom and $\vec{\zeta}_{B_m}$ is a vector which connects Li to the B_m carbon atom.

At the Γ point, $\gamma_6(0) = -\sqrt{6} t_1^{LiC}$ and $\gamma_i(0) = 0$ for $i = 1, \dots, 5$. These results show that just the isolated intercalant band, $E_{Li,0}(0)$ and the lowest valance band, $E_{sh,6}(0)$, are mutually affected. The energies of these bands are, with $E_0(0) \equiv E_+$, $E_6(0) \equiv E_-$,

$$E_{\pm}(0) = \frac{1}{2} (E_{Li,0}(0) + E_{sh,6}(0)) \pm \sqrt{\frac{1}{4} [E_{Li,0}(0) - E_{sh,6}(0)]^2 + 6(t_1^{LiC})^2} \quad (66)$$

and other shrunk graphene bands Eq. 39 remain unchanged. This means the energy gap at Γ , $E_g(0)$, depends only on the nearest neighbor hopping difference rather than on t_1^{LiC} . That is because the overlap between the Li s band and the valance band of uncoupled shrunk graphene (which is linear combination of s and f , $|\phi_6(0)\rangle$) is significant while others are zero.

For general \vec{k} vectors it is challenging to obtain an exact analytical expression for the full Hamiltonian in Eq. 25 and it would not be transparent anyway. One can use perturbation theory to obtain useful results. For $H_{ND} = H_{0D} + H_{1D}$ we can use non degenerate perturbation theory, obtaining

$$H_{ND}(\vec{k}) |\psi_N(E_i)\rangle = E_i(\vec{k}) |\psi_N(E_i)\rangle \quad (67)$$

where expansion of $E_i(\vec{k})$ in terms of perturbation parameter is $E_i(\vec{k}) = E_i^0(\vec{k}) + \mathcal{E}_i^1(\vec{k}) + \mathcal{E}_i^2(\vec{k}) + \dots$. From non degenerate perturbation we have

$$\mathcal{E}_i^1(\vec{k}) = \langle \phi_i | H_1 D | \phi_i \rangle, \quad \mathcal{E}_i^2(\vec{k}) = \sum_{j \neq i} \frac{|\langle \phi_i | H_1 D | \phi_j \rangle|^2}{E_i^0(\vec{k}) - E_j^0(\vec{k})} \quad (68)$$

where $|\phi_i\rangle$ is i th eigenstate of diagonal H_{0D} . Perturbed system eigenstates up to first order are

$$|\psi_N(E_i(\vec{k}))\rangle = |\phi_i(E_i^0(\vec{k}))\rangle + \sum_{j \neq i} \frac{1}{E_i^0 - E_j^0} |\phi_j^0(E_j(\vec{k}))\rangle. \quad (69)$$

Non degenerate perturbation theory can be used in Eq. 63 for completely filled or empty bands that are far from lithium band, $E_{Li,0}(\vec{k})$, and also without overlap. Therefore, except $E_{sh,2}$ and $E_{sh,3}$ which are nearly degenerate with lithium band in some regions, non degenerate approximation can be used for other bands of H_{0N} . We denote Hamiltonian in Eq. 63 as H_{DN} . This

Hamiltonian can be separated to $H_{ND} = H_{0D} + H_{1D}$ where

$$H_{0D} = \left(\begin{array}{c|cccccc} E_{Li,0}(\vec{k}) & 0 & \gamma_2(\vec{k}) & \gamma_3(\vec{k}) & 0 & 0 & 0 \\ \hline 0 & E_{sh,1}(\vec{k}) & 0 & 0 & 0 & 0 & 0 \\ \gamma_2^*(\vec{k}) & 0 & E_{sh,2}(\vec{k}) & 0 & 0 & 0 & 0 \\ \gamma_3^*(\vec{k}) & 0 & 0 & E_{sh,3}(\vec{k}) & 0 & 0 & 0 \\ 0 & 0 & 0 & 0 & E_{sh,4}(\vec{k}) & 0 & 0 \\ 0 & 0 & 0 & 0 & 0 & E_{sh,5}(\vec{k}) & 0 \\ 0 & 0 & 0 & 0 & 0 & 0 & E_{sh,6}(\vec{k}) \end{array} \right). \quad (70)$$

$$H_{1D} = \left(\begin{array}{c|cccccc} 0 & \gamma_1(\vec{k}) & 0 & 0 & \gamma_4(\vec{k}) & \gamma_5(k) & \gamma_6(\vec{k}) \\ \hline \gamma_1^*(\vec{k}) & 0 & 0 & 0 & 0 & 0 & 0 \\ 0 & 0 & 0 & 0 & 0 & 0 & 0 \\ 0 & 0 & 0 & 0 & 0 & 0 & 0 \\ \gamma_4^*(\vec{k}) & 0 & 0 & 0 & 0 & 0 & 0 \\ \gamma_5^*(\vec{k}) & 0 & 0 & 0 & 0 & 0 & 0 \\ \gamma_6^*(\vec{k}) & 0 & 0 & 0 & 0 & 0 & 0 \end{array} \right). \quad (71)$$

introducing below coefficients

$$\begin{aligned} c_2 &= E_{Li,0}(\vec{k}) + E_{sh,2}(\vec{k}) + E_{sh,3}(\vec{k}) \\ c_1 &= -(E_{Li,0}(\vec{k})E_{sh,2}(\vec{k}) + E_{Li,0}(\vec{k})E_{sh,3}(\vec{k}) + E_{sh,2}(\vec{k})E_{sh,3}(\vec{k}) - |\gamma_2(\vec{k})|^2 - |\gamma_3(\vec{k})|^2) \\ c_0 &= E_{Li,0}(\vec{k})E_{sh,2}(\vec{k})E_{sh,3}(\vec{k}) - E_{sh,3}(\vec{k})|\gamma_2(\vec{k})|^2 - E_{sh,2}(\vec{k})|\gamma_3(\vec{k})|^2 \\ \Pi &= (q + i\sqrt{p^3 - q^2}), \quad q = \frac{c_0}{2} + \frac{c_1 c_2}{6} + \frac{c_2^3}{27}, \quad p = \frac{c_1}{3} + \frac{c_2^2}{9} \end{aligned} \quad (72)$$

Non trivial eigenstate of H_{0D} are

$$E_0^0(\vec{k}) = \frac{c_2}{2} + \Pi + \Pi^*, \quad E_2^0(\vec{k}) = \frac{c_2}{2} + e^{i2\pi/3}\Pi + e^{-i2\pi/3}\Pi^*, \quad E_3^0(\vec{k}) = \frac{c_2}{2} + e^{-i2\pi/3}\Pi + e^{i2\pi/3}\Pi^* \quad (73)$$

and corresponding eigenstates are

$$\begin{aligned} |\phi_0(E_0^0(\vec{k}))\rangle &= (C_{p1}(E_0^0(\vec{k})) \ 0 \ C_{p2}(E_0^0(\vec{k}))C_{p3}(E_0^0(\vec{k}))0 \ 0 \ 0)^T \\ |\phi_2(E_2^0(\vec{k}))\rangle &= (C_{p1}(E_2^0(\vec{k})) \ 0 \ C_{p2}(E_2^0(\vec{k}))C_{p3}(E_2^0(\vec{k}))0 \ 0 \ 0)^T \\ |\phi_3(E_3^0(\vec{k}))\rangle &= (C_{p1}(E_3^0(\vec{k})) \ 0 \ C_{p2}(E_3^0(\vec{k}))C_{p3}(E_3^0(\vec{k}))0 \ 0 \ 0)^T \end{aligned} \quad (74)$$

It is easy to show that $\mathcal{E}_1^0 = 0$. So up to second order perturbation parameter the eigenenergies are

$$\begin{aligned}
E_0(\vec{k}) &= E_0^0(\vec{k}) - |C_{p1}(E_0^0)|^2 \left(\frac{|\gamma_1|^2}{E_{sh,1} - E_0^0} + \frac{|\gamma_4|^2}{E_{sh,4} - E_0^0} + \frac{|\gamma_5|^2}{E_{sh,5} - E_0^0} + \frac{|\gamma_6|^2}{E_{sh,6} - E_0^0} \right) \\
E_1(\vec{k}) &= E_{sh,1}(\vec{k}) + |C_{p1}(E_0^0)|^2 \frac{|\gamma_1|^2}{E_{sh,1} - E_0^0} + |C_{p1}(E_2^0)|^2 \frac{|\gamma_1|^2}{E_{sh,1} - E_2^0} + |C_{p1}(E_3^0)|^2 \frac{|\gamma_1|^2}{E_{sh,1} - E_3^0} \\
E_2(\vec{k}) &= E_2^0(\vec{k}) - |C_{p1}(E_2^0)|^2 \left(\frac{|\gamma_1|^2}{E_{sh,1} - E_2^0} + \frac{|\gamma_4|^2}{E_{sh,4} - E_2^0} + \frac{|\gamma_5|^2}{E_{sh,5} - E_2^0} + \frac{|\gamma_6|^2}{E_{sh,6} - E_2^0} \right) \\
E_3(\vec{k}) &= E_3^0(\vec{k}) - |C_{p1}(E_3^0)|^2 \left(\frac{|\gamma_1|^2}{E_{sh,1} - E_3^0} + \frac{|\gamma_4|^2}{E_{sh,4} - E_3^0} + \frac{|\gamma_5|^2}{E_{sh,5} - E_3^0} + \frac{|\gamma_6|^2}{E_{sh,6} - E_3^0} \right) \\
E_4(\vec{k}) &= E_{sh,4}(\vec{k}) + |C_{p1}(E_0^0)|^2 \frac{|\gamma_4|^2}{E_{sh,4} - E_0^0} + |C_{p1}(E_2^0)|^2 \frac{|\gamma_4|^2}{E_{sh,4} - E_2^0} + |C_{p1}(E_3^0)|^2 \frac{|\gamma_4|^2}{E_{sh,4} - E_3^0} \\
E_5(\vec{k}) &= E_{sh,5}(\vec{k}) + |C_{p1}(E_0^0)|^2 \frac{|\gamma_5|^2}{E_{sh,5} - E_0^0} + |C_{p1}(E_2^0)|^2 \frac{|\gamma_5|^2}{E_{sh,5} - E_2^0} + |C_{p1}(E_3^0)|^2 \frac{|\gamma_5|^2}{E_{sh,5} - E_3^0} \\
E_6(\vec{k}) &= E_{sh,6}(\vec{k}) + |C_{p1}(E_0^0)|^2 \frac{|\gamma_6|^2}{E_{sh,6} - E_0^0} + |C_{p1}(E_2^0)|^2 \frac{|\gamma_6|^2}{E_{sh,6} - E_2^0} + |C_{p1}(E_3^0)|^2 \frac{|\gamma_6|^2}{E_{sh,6} - E_3^0}
\end{aligned} \tag{75}$$

D Bogoliubov-de Gennes Transformation

The electron-electron interaction part of Hamiltonian, H_P , in the mean field approximation becomes

$$\hat{H}_P^{MF} = \frac{1}{2} \sum_{i\alpha\sigma} \sum_{j\beta\sigma'} \Delta_{i\alpha,j\beta}^{\sigma\sigma'} \hat{c}_{i\alpha\sigma}^\dagger \hat{c}_{j\beta\sigma'}^\dagger + h.c. + F_0 = \frac{1}{2} \sum_{\vec{k}\alpha\sigma\beta\sigma'} \Delta_{\alpha\beta}^{\sigma\sigma'}(\vec{k}) \hat{c}_{\alpha\sigma}^\dagger(\vec{k}) \hat{c}_{\beta\sigma'}^\dagger(-\vec{k}) + h.c. + F_0 \tag{76}$$

in which $\Delta_{i\alpha,j\beta}^{\sigma\sigma'} = U_{i\alpha,j\beta}^{\sigma\sigma'} \langle \hat{c}_{i\alpha\sigma} \hat{c}_{j\beta\sigma'} \rangle$ is the matrix of order parameters in real space. Fourier transformation of real space order parameters are given by

$$\Delta_{\alpha\beta}^{\sigma\sigma'}(\vec{k}) = \frac{1}{N} \sum_{ij} \Delta_{i\alpha,j\beta}^{\sigma\sigma'} e^{i\vec{k} \cdot (\vec{r}_{i\alpha} - \vec{r}_{j\beta})}. \tag{77}$$

here Latin subscripts, α and β refers to A_i or B_i subsites. The interacting Hamiltonian in Nambu space is

$$\hat{H}_{SU} = \sum_{\vec{k}} \hat{\Psi}^\dagger(\vec{k}) H_{SU}(\vec{k}) \hat{\Psi}(\vec{k}) \tag{78}$$

where $\hat{\Psi}^\dagger(\vec{k}) = (c_{0\uparrow}^\dagger(\vec{k}), c_{1\uparrow}^\dagger(\vec{k}), \dots, c_{6\uparrow}^\dagger(\vec{k}), c_{0\downarrow}(-\vec{k}), c_{1\downarrow}(-\vec{k}), \dots, c_{6\downarrow}(-\vec{k}))$ where $Li, A_1, A_2, A_3, B_1, B_2$ and B_3 are labeled by 0, 1, 2, 3, 4, 5, 6 respectively, and

$$H_{SU}(\vec{k}) = \begin{pmatrix} H_N(\vec{k}) & H_P(\vec{k}) \\ H_P^\dagger(\vec{k}) & -H_N^*(-\vec{k}) \end{pmatrix}. \tag{79}$$

The coupling is given by

$$H_P(\vec{k}) = \begin{pmatrix} 0 & 0 & 0 & 0 & 0 & 0 & 0 \\ 0 & 0 & 0 & 0 & \Delta_{A_1 B_1}^{\uparrow\downarrow}(\vec{k}) & \Delta_{A_1 B_2}^{\uparrow\downarrow}(\vec{k}) & \Delta_{A_1 B_3}^{\uparrow\downarrow}(\vec{k}) \\ 0 & 0 & 0 & 0 & \Delta_{A_2 B_1}^{\uparrow\downarrow}(\vec{k}) & \Delta_{A_2 B_2}^{\uparrow\downarrow}(\vec{k}) & \Delta_{A_2 B_3}^{\uparrow\downarrow}(\vec{k}) \\ 0 & 0 & 0 & 0 & \Delta_{A_3 B_1}^{\uparrow\downarrow}(\vec{k}) & \Delta_{A_3 B_2}^{\uparrow\downarrow}(\vec{k}) & \Delta_{A_3 B_3}^{\uparrow\downarrow}(\vec{k}) \\ 0 & \Delta_{A_1 B_1}^{\uparrow\downarrow*}(\vec{k}) & \Delta_{A_2 B_1}^{\uparrow\downarrow*}(\vec{k}) & \Delta_{A_3 B_1}^{\uparrow\downarrow*}(\vec{k}) & 0 & 0 & 0 \\ 0 & \Delta_{A_1 B_2}^{\uparrow\downarrow*}(\vec{k}) & \Delta_{A_2 B_2}^{\uparrow\downarrow*}(\vec{k}) & \Delta_{A_3 B_2}^{\uparrow\downarrow*}(\vec{k}) & 0 & 0 & 0 \\ 0 & \Delta_{A_1 B_3}^{\uparrow\downarrow*}(\vec{k}) & \Delta_{A_2 B_3}^{\uparrow\downarrow*}(\vec{k}) & \Delta_{A_3 B_3}^{\uparrow\downarrow*}(\vec{k}) & 0 & 0 & 0 \end{pmatrix} \tag{80}$$

for singlet $\Delta_{\beta\alpha}^{\uparrow\downarrow}(\vec{k}) = \Delta_{\alpha\beta}^{\uparrow\downarrow}(-\vec{k}) = -\Delta_{\alpha\beta}^{\uparrow\downarrow}(-\vec{k}) = \Delta_{\alpha\beta}^{\uparrow\downarrow*}(\vec{k})$. The order parameters according to (main text) Fig. 4 are

$$\begin{aligned}\Delta_{A_1B_1}^{\uparrow\downarrow}(\vec{k}) &= \Delta_1'' e^{i\vec{k}\cdot\vec{\tau}_1}, \quad \Delta_{A_1B_2}^{\uparrow\downarrow}(\vec{k}) = \Delta_2 e^{i\vec{k}\cdot\vec{\delta}_2}, \quad \Delta_{A_1B_3}^{\uparrow\downarrow}(\vec{k}) = \Delta_3' e^{i\vec{k}\cdot\vec{\delta}_3}; \\ \Delta_{A_2B_1}^{\uparrow\downarrow}(\vec{k}) &= \Delta_2' e^{i\vec{k}\cdot\vec{\delta}_2}, \quad \Delta_{A_2B_2}^{\uparrow\downarrow}(\vec{k}) = \Delta_3'' e^{i\vec{k}\cdot\vec{\tau}_3}, \quad \Delta_{A_2B_3}^{\uparrow\downarrow}(\vec{k}) = \Delta_1 e^{i\vec{k}\cdot\vec{\delta}_1}; \\ \Delta_{A_3B_1}^{\uparrow\downarrow}(\vec{k}) &= \Delta_3 e^{i\vec{k}\cdot\vec{\delta}_3}, \quad \Delta_{A_3B_2}^{\uparrow\downarrow}(\vec{k}) = \Delta_1' e^{i\vec{k}\cdot\vec{\delta}_1}, \quad \Delta_{A_3B_3}^{\uparrow\downarrow}(\vec{k}) = \Delta_2'' e^{i\vec{k}\cdot\vec{\tau}_2}.\end{aligned}\quad (81)$$

$U_{<iA_1\uparrow jB_1\downarrow>} = U_{<iA_2\uparrow jB_2\downarrow>} = U_{<iA_3\uparrow jB_3\downarrow>} g_1$ Quasiparticle energies are obtained by unitary transformation in the seven band space

$$\hat{H}_{SU} = \sum_{\vec{k}} \hat{\Psi}^\dagger(\vec{k}) Q \left[Q^\dagger H_{SU}(\vec{k}) Q \right] Q^\dagger \hat{\Psi}(\vec{k}) = \sum_{\vec{k}} \Lambda^\dagger(\vec{k}) H_{SU}^N(\vec{k}) \Lambda(\vec{k}) \quad (82)$$

where in matrix notation,

$$H_{SU}^N(\vec{k}) = \begin{pmatrix} H_{ND}(\vec{k}) & H_{PD}(\vec{k}) \\ H_{PD}^\dagger(\vec{k}) & -H_{ND}^*(-\vec{k}) \end{pmatrix}, \quad Q = \begin{pmatrix} \hat{P}_N(\vec{k}) & \hat{0} \\ \hat{0} & \hat{P}_N^*(-\vec{k}) \end{pmatrix}. \quad (83)$$

$\hat{P}_N(\vec{k})$ is a 7×7 matrix where each column is one of the perturbed normal state eigenvectors of Eq. 25, thus with matrix elements given by $[\hat{P}_N^\dagger]_{i,j} = \mathcal{C}_i(E_j(\vec{k}))$. $H_{ND}(\vec{k})$ is the corresponding diagonal seven band Hamiltonian. Here $\hat{P}_N^*(-\vec{k}) = \hat{P}_N(\vec{k})$. In the normal band space the matrix elements of the off-diagonal array are given by

$$[H_{DP}(\vec{k})]_{i,j} = \Delta_{ij}(\vec{k}) = \sum_{\alpha=1}^9 \Omega_{ij}^\alpha(\vec{k}) \Delta^\alpha \quad (84)$$

Using the fact that the gap is small, applying perturbation up to second order in the order parameter gives quasiparticle energies

$$E_{m,s}^Q(\vec{k}) = s \left(E_m(\vec{k}) + \sum_{i=1}^7 \frac{|\Delta_{mi}(\vec{k})|^2}{E_m(\vec{k}) + E_i(\vec{k})} \right) \quad s = \pm 1 \quad (85)$$

where $s = 1$ is for particles and $s = -1$ for holes.

E Superconducting States

By minimizing the quasiparticle free energy with respect to nearest neighbor order parameters the gap equation is obtained. The free energy is

$$F = -\frac{2}{\beta} \sum_{\vec{k}} \sum_{n=1}^7 \ln \left[2 \cosh \left(\frac{E_n^Q}{2k_B T} \right) \right] + F_0. \quad (86)$$

where F_0 is the system condensation energy,

$$F_0 = -\frac{1}{2} \sum_{i\alpha\sigma} \sum_{j\beta\sigma'} \Delta_{i\alpha j\beta}^{\sigma\sigma'} G_{i\alpha j\beta}^{\sigma\sigma'} = -2N \sum_{\alpha=1}^9 J_\alpha (\Delta^\alpha)^2 \quad (87)$$

where $J_1 = J_2 = J_3 = \frac{1}{g_1}$ and $J_4 = J_5 = J_6 = J_7 = J_8 = J_9 = \frac{1}{g_0}$. The linearized gap equation, obtained by minimizing free energy of the system, is

$$J_\beta \Delta^\beta = -\frac{1}{2N} \sum_{\alpha=1}^9 \left[\sum_{\vec{k}} \sum_{n=1}^7 \sum_{i=1}^7 \frac{\tanh(\frac{E_n^Q}{2k_B T})}{E_n(\vec{k}) + E_i(\vec{k})} \left(\Omega_{ni}^\alpha(\vec{k}) \Omega_{ni}^{*\beta}(\vec{k}) + \Omega_{ni}^\beta(\vec{k}) \Omega_{ni}^{*\alpha}(\vec{k}) \right) \right] \Delta^\alpha \equiv -\sum_{\alpha=1}^9 \Gamma_{\beta\alpha} \Delta^\alpha. \quad (88)$$

We have used that at T_c , where $|\Delta_{ij}|^2$ can be neglected, $E_n^Q \rightarrow E_n$.

In the general case, (see main text Fig. 4), the system is invariant under interchange $2 \rightleftharpoons 5$, $3 \rightleftharpoons 6$ and $4 \rightleftharpoons 7$, which means $\Delta_i' \rightleftharpoons \Delta_i$. These relations correspond to $\Delta^4 \rightleftharpoons \Delta^7$, $\Delta^5 \rightleftharpoons \Delta^8$ and $\Delta^6 \rightleftharpoons \Delta^9$ in Eq. 88. This symmetry and that of the symmetric Γ matrix $\Gamma_{\beta\alpha} = \Gamma_{\alpha\beta}$ allows Eq. 88 to be written in matrix form as

$$\begin{bmatrix} A_{3 \times 3} & B_{3 \times 3} & B_{3 \times 3} \\ B_{3 \times 3} & C_{3 \times 3} & D_{3 \times 3} \\ B_{3 \times 3} & D_{3 \times 3} & C_{3 \times 3} \end{bmatrix} \begin{pmatrix} g_1 V_1 \\ g_0 V_2 \\ g_0 V_3 \end{pmatrix} = - \begin{pmatrix} V_1 \\ V_2 \\ V_3 \end{pmatrix} \quad (89)$$

where

$$A_{3 \times 3} = \begin{bmatrix} \Gamma_{11} & \Gamma_{12} & \Gamma_{12} \\ \Gamma_{12} & \Gamma_{11} & \Gamma_{12} \\ \Gamma_{12} & \Gamma_{12} & \Gamma_{11} \end{bmatrix}, C_{3 \times 3} = \begin{bmatrix} \Gamma_{44} & \Gamma_{45} & \Gamma_{45} \\ \Gamma_{45} & \Gamma_{44} & \Gamma_{45} \\ \Gamma_{45} & \Gamma_{45} & \Gamma_{44} \end{bmatrix}, B_{3 \times 3} = \begin{bmatrix} \Gamma_{14} & \Gamma_{15} & \Gamma_{15} \\ \Gamma_{15} & \Gamma_{14} & \Gamma_{15} \\ \Gamma_{15} & \Gamma_{15} & \Gamma_{14} \end{bmatrix}, D_{3 \times 3} = \begin{bmatrix} \Gamma_{47} & \Gamma_{48} & \Gamma_{48} \\ \Gamma_{48} & \Gamma_{47} & \Gamma_{48} \\ \Gamma_{48} & \Gamma_{48} & \Gamma_{47} \end{bmatrix} \quad (90)$$

Eq. 89 can be written as a non-Hermitian eigenvalue problem

$$\begin{bmatrix} \kappa A & \kappa B & \kappa B \\ B & C & D \\ B & D & C \end{bmatrix} \begin{pmatrix} g_1 V_1 \\ g_0 V_2 \\ g_0 V_3 \end{pmatrix} = -\frac{1}{g_0} \begin{pmatrix} g_1 V_1 \\ g_0 V_2 \\ g_0 V_3 \end{pmatrix} \quad (91)$$

where $\kappa = \frac{g_1}{g_0}$. Substates V_1 , V_2 and V_3 in gap equation Eq. 91, cannot have different symmetries, so each of the eigenvectors of Eq. 91 can be expressed in the compact form

$$[\Phi_n]^T = [\alpha_{sy} V_{sy} \quad \beta_{sy} V_{sy} \quad \gamma_{sy} V_{sy}] \quad (92)$$

where subscript sy refers to one of the s -wave, d_{xy} -wave or $d_{x^2-y^2}$ -wave symmetries, and the coefficients α_{sy} , β_{sy} and γ_{sy} are to be determined. By inserting eigenvectors from Eq. 92 into the gap equation Eq. 91 one finds

$$\frac{\alpha_{sy}}{\beta_{sy}} = \frac{\alpha_{sy}}{\gamma_{sy}}, \quad \frac{\gamma_{sy}}{\beta_{sy}} = \frac{\beta_{sy}}{\gamma_{sy}}, \quad J_{sy} = c_{sy} + \frac{\beta_{sy}}{\gamma_{sy}} d_{sy} + \frac{\alpha_{sy}}{\gamma_{sy}} b_{sy} \quad (93)$$

where $c_{sy} = c_s, c_d$, $b_{sy} = b_s, b_d$, $d_{sy} = d_s, d_d$ and $J_{sy} = -\frac{1}{g_0}$ for each symmetry. Eq. 93 has two classes of solutions

$$\begin{aligned} \beta_{sy} &= -\gamma_{sy} \equiv 1 \Rightarrow \alpha_{sy} = 0, \quad J_{sy}^0 = c_{sy} - d_{sy}, \\ \beta_{sy} &= +\gamma_{sy} \equiv 1 \Rightarrow b_{sy} \alpha_{sy}^2 + (c_{sy} + d_{sy} - \kappa a_{sy}) \alpha_{sy} - 2\kappa b_{sy} = 0 \end{aligned} \quad (94)$$

In the limiting case of pristine graphene, the quadratic equation in Eq. 94, has two temperature independent solutions $\alpha_{sy} = 1$ and $\alpha_{sy} = -2$. The last solution in addition to island states $\alpha_{sy} = 0$ are in fact, orthogonal states where they are linear combination of the aforementioned Φ_{0n} and Φ_{1n} . But in the general case of symmetry breaking LiC₆ characterized by gap equation Eq. 89, the quadratic equation in Eq. 94, has two temperature dependent solutions,

$$\alpha_{sy}^{\pm} = \frac{J_{sy}^{\pm} - c_{sy} - d_{sy}}{b_{sy}}, \quad J_{sy}^{\pm} = \frac{1}{2} \left(\kappa a_{sy} + c_{sy} + d_{sy} \pm \sqrt{8\kappa b_{sy}^2 + [c_{sy} + d_{sy} - \kappa a_{sy}]^2} \right) \quad (95)$$

| n | 0 | 1 | 2 | 3 | 4 | 5 | 6 | 7 | 8 | 9 |
|-----------------|-----------------------|--------------|------------------|---------------|------------------|--------------|--------------------|---------------|--------------------|---------------|
| t_{0n}^{CC} | $\epsilon_c = -0.77$ | $t_1 = 2.93$ | $t'_1 = 0.94t_1$ | $t_2 = -0.22$ | $t'_2 = 0.94t_2$ | $t_3 = 0.28$ | $t'_3 \approx t_3$ | $t_4 = -0.03$ | $t'_4 \approx t_4$ | $t_5 = -0.05$ |
| m | 0 | 1 | 2 | 3 | 4 | | | | | |
| t_{0m}^{LiLi} | $\epsilon_{Li} = 1.1$ | -0.30 | 0.09 | 0.04 | -0.03 | | | | | |
| t_{0m}^{LiC} | — | 0.30 | | | | | | | | |

Table 1. The C-C hopping parameters (eV) for LiC₆ are denoted by t_{0n}^{CC} where the index n indicates n -th neighbours. In the Li plane, Li-Li hopping parameters are denoted by t_{0m}^{LiLi} where m is m -th Li neighbor of central Li. The Li-C hopping parameter is t_{0m}^{LiC} .

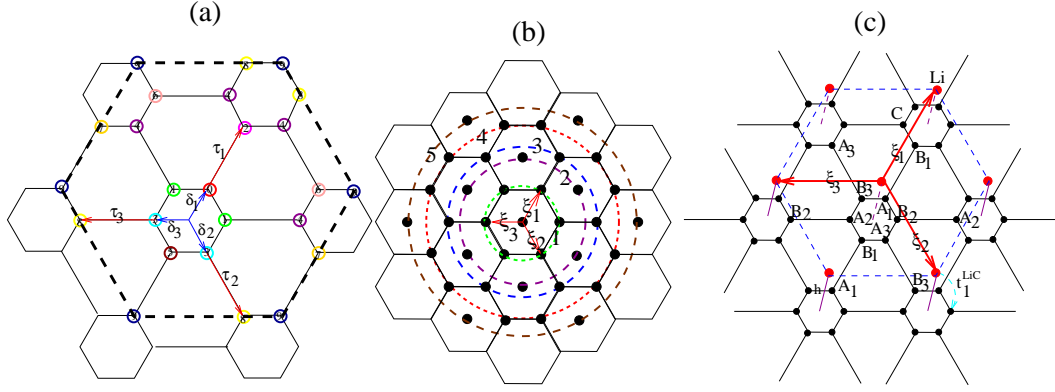


Figure 1. (Color online) (a) Schematic diagram of the shrunk graphene lattice, with the distortion emphasized. (b) The hexagonal Li sheet, indicating the circles that Li neighbors lie on. (c) Diagram of the graphene decorated by lithium. The red Li atoms lie above the centers of the C hexagons.

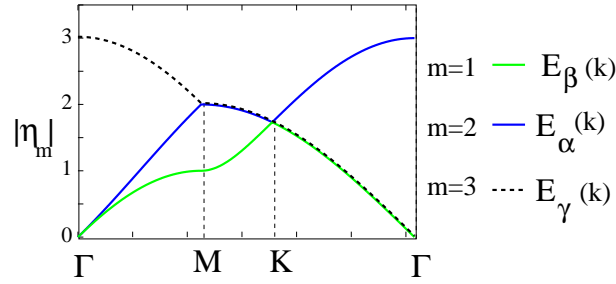


Figure 2. (Color online) A plot of the dispersion expressions $|\eta_m(\vec{k})|$, the three folded branches of pristine π^* band structure in the mini-Brillouin zone of graphene C_6 . The Bloch wave character of E_β is $f_d^1|d-ip\rangle + f_p^1|p-id\rangle$, of the E_α is $f_d^2|d+ip\rangle + f_p^2|p+id\rangle$ and for E_γ is $f_s|s\rangle + f_f|f\rangle$. Here we use abbreviated notation $f_d^{1(2)}|d \pm ip\rangle = f_{d_{x^2-y^2}}^{1(2)}(|d_{x^2-y^2} \rangle \pm i|p_x \rangle)$ and $f_p^{1(2)}|p \pm id\rangle = f_{p_y}^{1(2)}(|p_y \rangle \pm i|d_{xy} \rangle)$

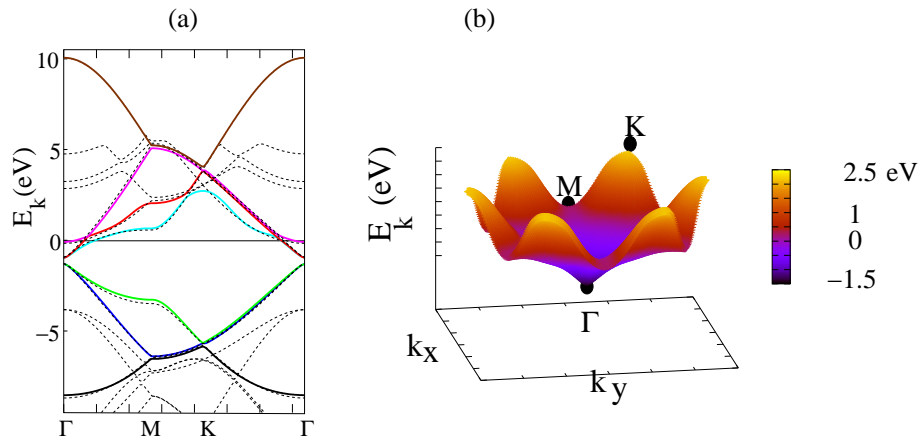


Figure 3. (Color online) The left panel provides the band structure of lithium decorated graphene. The dashed lines indicate the DFT bands, while the fitted bands are shown in color. The Fermi energy set to zero at $\mu_0 = 0.4\text{eV}$. A small gap, $E_g = 0.36\text{eV}$ is opened at the Γ point around -1.12eV . The right panel provides a surface plot of the relatively flat band of LiC_6 . d -wave pairing dominates due to electrons in the valleys around saddle points at M .

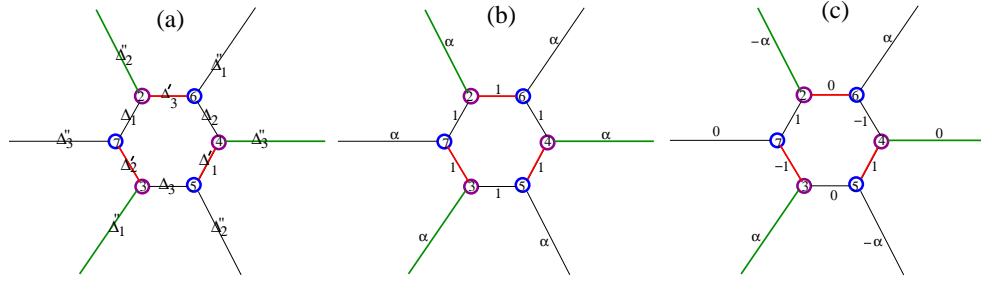


Figure 4. (Color online) (a) Designation of the pairing amplitudes considered in this study, which cover all nearest neighbor pairing possibilities denoted by $\Delta_{n<ij>}$, $\Delta'_{n<ij>}$ and $\Delta''_{n<ij>}$ where subscript $<ij>$ has been dropped for brevity. (b) shows the pairing amplitude for Φ_S^+ phase with $\alpha \approx 0.6$ and for Φ_S^- phase with $\alpha \approx -3.4$. Both phases broken two band graphene symmetry as can be seen by comparing symmetries along different bonds in seven atoms unit cell and two bands unit cell where its Bravais lattice points are labeled by 5, 6 and 7. (c) shows the pairing amplitude $\Phi_{d_{xy}}^+$ where $\alpha \approx 1$ and $\Phi_{d_{xy}}^-$ where $\alpha \approx -2$. The first phase approximately preserves two band graphene symmetry while the others arise from broken symmetry.

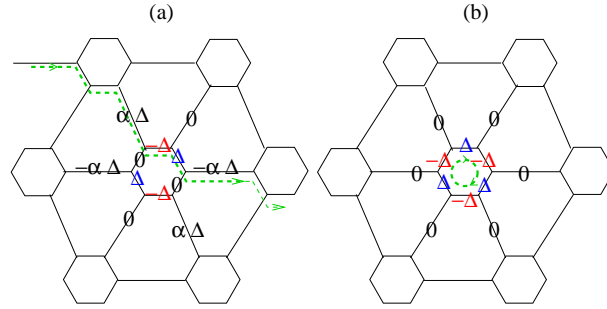


Figure 5. (Color online) Schematic diagram illustrating Cooper pair propagation for (a) Φ_{xy}^f along a chain as shown by the green dashed line and arrow, and (b) localized “island” pairs for Φ_f .

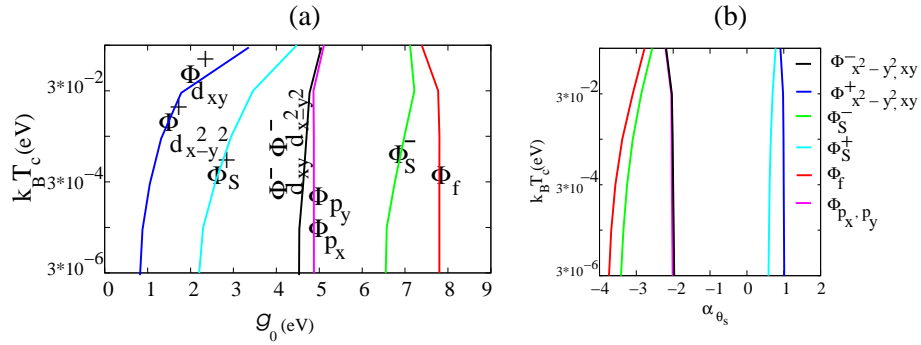


Figure 6. (Color on line) (a) This phase diagram illustrates the relation between T_c and the pairing potential g_0 for LiC_6 in which $\mu_0 = 0$. Panel (b) shows T_c in terms of α_{xy}

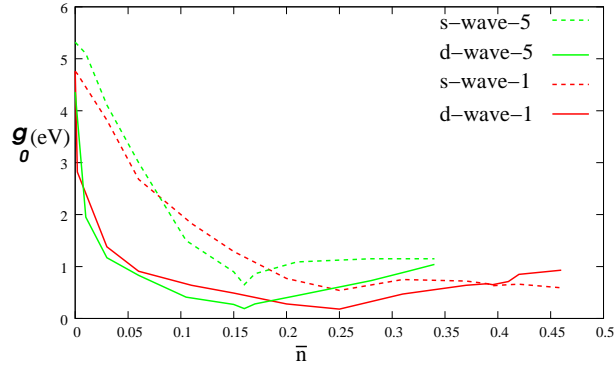


Figure 7. (Color online) shows cooper pair interaction g_0 in terms of doping \bar{n} for d and s-wave phases for pristine graphene at $T = 0.1\text{K}$. The solid (dashed) red line indicates d- wave (s- wave) pairing interaction in first nearest neighbor hopping $t_1 = 2.5eV$ and similarly green line for accurate tight binding model can fit on DFT. For red line at the charge neutrality s- and d- wave are degenerate with $g_0 = 4.76$ while for full approximation they are not degenerate.

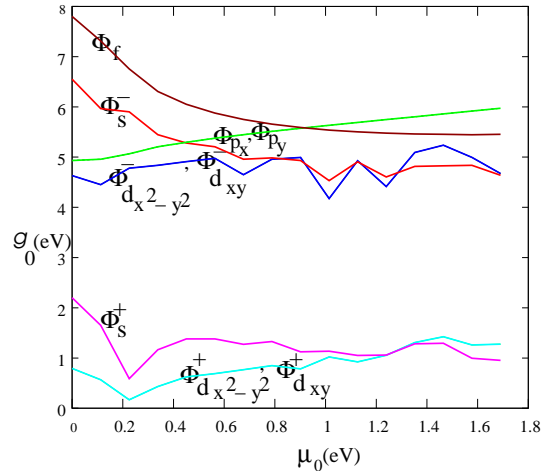


Figure 8. (Color online) This diagram illustrates interaction potential g_0 in terms of chemical potential μ_0 at $T_c = 0.1\text{ K}$. Upon electron doping to a critical chemical potential $\mu_{o-v} = 0.22\text{eV}$ (van Hove singularity) for symmetries $\Phi_{d_{x^2-y^2}}^+$, $\Phi_{d_{xy}}^+$, and Φ_s^+ the pairing potential decreases, then increases until a second critical value $\mu_{o-c} = 1.3\text{ eV}$ at which a phase transition to Φ_s^+ occurs.